An innovative framework for real-time monitoring of pollutant point sources in river networks

An Innovative Framework for Real Time Monitoring of Pollutant Point Sources in River Networks

M. BaratiMoghaddam
Tarbiat Modares University https://orcid.org/0000-0001-8346-1707
Mehdi Mazaheri (m.mazaheri@modares.ac.ir)
Tarbiat Modares University https://orcid.org/0000-0001-8670-1710
J. M. V. Samani
Tarbiat Modares University
Fulvio Boano
Politecnico di Torino

Research Article

Keywords: Geostatistical approach, Inverse problem, Multiple pollutant point sources, Source identification, Unsteady flow, River network

Posted Date: June 18th, 2021

DOI: https://doi.org/10.21203/rs.3.rs-597673/v1

An Innovative Framework for Real Time Monitoring of Pollutant Point Sources in River Networks

M. BaratiMoghaddam[1, 2], M. Mazaheri[1*], J. M. V. Samani[1] and F. Boano[2]

[1] Department of Water Engineering and Management, Tarbiat Modares University, Tehran, Iran.

[2] Department of Environment, Land and Infrastructure Engineering (DIATI), Politecnico di Torino, Turin, Italy.

[*] Corresponding author: m.mazaheri@modares.ac.ir

An Innovative Framework for Real Time Monitoring of Pollutant Point Sources in River Networks

Abstract:

The simultaneous identification of location and source release history in complex river networks is a very complicated ill-posed problem, particularly in a case of multiple unknown pollutant sources with time-varying release pattern. This study presents an innovative method for simultaneous identification of the number, locations and release histories of multiple pollutant point sources in a river network using minimum observation data. Considering two different type of monitoring stations with an adaptive arrangement as well as real-time data collection at those stations and using a reliable numerical flow and transport model, at first the number and suspected reach of presence of pollutant sources are determined. Then the source location and its intensity function is calculated by solving inverse source problem using a geostatistical approach. A case study with three different scenarios in terms of the number, release time and location of pollutant sources are discussed, concerning a river network with unsteady and non-uniform flow. Results showed the capability of the proposed method in identifying of sought source characteristics even in complicated cases with simultaneous activity of multiple pollutant sources.

Keywords: Geostatistical approach, Inverse problem, Multiple pollutant point sources, Source identification, Unsteady flow, River network.

1. Introduction

Water resources are essential to life on the Earth planet, but these limited and valuable resources are increasingly under threat. Rivers in particular due to proximity to big cities and extensive usage in industrial and agricultural activities, are extremely exposed to accidental or intentional spills. Regarding to this issue, in recent years, a great attention has been drawn to simulate fate and transport of contaminants in rivers as well as to identify pollutant sources characteristics. Recovering release history of pollutant sources is essential in planning effective remediation strategies. Moreover, determining the number and location of pollutant sources is of great importance in order to identify responsible parties for observed pollution cloud in downstream and divide remediation measure expenses among those parties (Skaggs and Kabala, 1994, Liu and Ball, 1999, Atmadja and Bagtzoglou, 2001, Michalak, 2002).

Given known concentration data at limited downstream observation points, the pollutant source identification problem is categorized as an inverse problem. Like most of the inverse problems, the inverse source problem does not fulfill the well-posedness criteria of Hadamard (1923). Based on Hadamard's definition, a problem is well-posed if its solution is existent, unique and stable. A problem which lacks any of these features called an ill-posed problem. However, since the observed pollution cloud at the downstream point, must be originated from somewhere at the upstream, pollutant source identification problem always has a solution and nonexistence would not raise an issue. Hence, there are two main challenges in solving an inverse source problem, namely nonuniqueness and instability of the solution. The nonuniqueness means that different combinations of intensity functions of the pollution sources at the upstream can create a single concentration-time curve at a given observation point downstream. Since time discretization of governing equation to pollution transport results in a system of equations which has fewer equations (observations) than unknowns (source values), multiple combinations for source characteristics might be detected which are consistent with

observed concentration data. To address the nonuniqueness issue researchers often assume that some prior information about the unknown source is available (e.g. possible location, activity duration or known intensity function, as well as, consideration a particular form of the source term function). The instability issue implies to large errors in the solution following small errors in measured data. It is mainly a consequence of irreversibility of dispersion phenomena, which gradually smooth the pollution plume and decrease the amount of obtainable information from observational data (Skaggs and Kabala, 1998). Hence, considering uncertainties in observed data regarding to measurement errors and sparsity of data increases the reliability of the identification results.

In the last 30 years, various methods have been proposed to solve pollutant source identification problem in surface and groundwater which can be broadly categorized into three classes: optimization-based approaches, stochastic-based approaches and mathematics-based approaches. A review of those research can be found in (Atmadja and Bagtzoglou, 2001, Michalak and Kitanidis, 2004b, Morrison, 2000b, Morrison, 2000a, Neupauer et al., 2000). Among these methods, stochastic-based methods are becoming a trend in solving inverse source problem in recent years. The most significant feature of stochastic-based approaches is to treat unknown pollution source parameters as random variables and use of probability distribution functions to predict those parameters. This feature provides the possibility of estimation of the source characteristics in greater number of instants than available observation data as well as consideration of uncertainty due to error in those data (Woodbury et al. 1998).

One of the stochastic-based methods which is extensively used in solving of inverse source problem in groundwater is Geostatistical (GS) method. The main assumption of GS method is that the unknown source function is random with a known correlation structure but unknown correlation structural parameters. The optimal values of these structural parameters are obtained using the geostatistical inversion theory presented by Kitanidis (1996) and the source

function recovered by minimizing a likelihood function while retaining the assumed correlation structure. More details can be found in Kitanidis (1995, 1996) and Snodgrass and Kitanidis (1997). The GS approach has been widely tested and improved in groundwater source identification through hypothetical cases (Snodgrass and Kitanidis, 1997, Michalak and Kitanidis, 2003, Michalak and Kitanidis, 2004b, Butera et al., 2013) and using field data (Michalak and Kitanidis, 2002, Michalak and Kitanidis, 2004a, Gzyl et al., 2014). This approach also had been applied only once in pollutant source identification in single-branched rivers considering the effects of transient storage zone as well as linear decay processes (Boano et al., 2005). Snodgrass and Kitanidis (1997) applied the GS approach for estimating the release history of a conservative solute in a 1D homogeneous aquifer. Instead of using the usual iterative techniques to obtain the best estimation of parameters, they combined GS techniques with Bayesian theory, which provides the possibility to quantify the estimation error. Michalak and Kitanidis (2002) applied the proposed approach by Snodgrass and Kitanidis (1997) for the reconstruction of the contaminant release history for a 3D plume at Gloucester landfill site in Ontario, Canada. Michalak and Kitanidis (2004b) combined the adjoint model with geostatistical techniques in order to reduce the computational cost as well as providing the possibility to use the approach in heterogeneous fields. In addition, using an adjoint model provides the feasibility of application of the existing groundwater flow and transport commercial codes in the framework of the proposed inverse method. Butera et al. (2013) based on GS proposed a framework for simultaneous identification of location and release history of a single pollutant source in 2D confined aquifers with strongly non-uniform flow field. Gzyl et al. (2014) presented a multi-step method based on performing an integral pumping test and GS approach to identify location and release history of a pollutant source in groundwater. The results of applying this method to a complicated contamination case at the adjacent reach to an abandoned chemical plant in southern Poland, indicated that it is able to successfully detect

suspected areas. However, the proposed methods by Butera et al. (2013) and Gzyl et al. (2014) need the prior knowledge of the approximate location of pollutant source at the beginning of a simulation, which is a challenge in practical applications, especially in complicated cases that such information may not be available.

Compared to numerous studies on pollutant source identification of in groundwater, only relatively few studies on solving an inverse source problem in surface waters can be found in literature (El Badia and Hamdi, 2007, Hamdi, 2009, Hamdi, 2016, Andrle and El Badia, 2012, Cheng and Jia, 2010, Mazaheri et al., 2015, Yang et al., 2016, Wang et al., 2018). While, the pollutant transport in rivers tends to be more advection-dominated than groundwater and, subsequently pollutant substance transported faster and further, which may lead to partial capturing of the pollution plume at the observation points. Thus, fast and accurate identification of illegal spills is more important in these environments to provide scientific support for planning mitigation and adaptation strategies. Furthermore, the research of pollutant source identification problem in surface waters was mainly confined to single-branch rivers and rarely involved river networks. This is mainly due to hydrodynamical complexity of such systems which along with inherent ill- posedness of corresponding source identification problem, form a problem that is very difficult to solve. However, regarding that tributaries in a river network usually are less monitored, those areas might be considered as potential places for illegal discharge of pollutants. Therefore, to prevent further damage, it is necessary to pay more attention to identifying pollutant sources characteristics in such environments.

Focusing on pollutant source identification in river networks, Telci and Aral (2011) by using an adaptive sequential feature selection algorithm (Jiang, 2008), determined the location of a single instantaneous source among several candidate locations. However, their proposed method requires a significant amount of simulation time for training monitoring stations with a large number of spill scenarios. Ghane et al. (2016) applied the backward probability method

144 to identify the source location and the released time of a single spill in a river system. Lee et
145 al. (2018) dealt with the problem of identifying the location of a single instantaneous source
146 via analyzing changes in concentration levels that observed by a sensor network in a river
147 system. By constructing random forest models, they determined the possibility that each
148 candidate location be the correct one as a number between zero and one. However, all of
149 mentioned studies considered a single pollutant source with a simple form of release (i.e. the
150 spill), while in many practical application, there are more than one active source and the release
151 functions varies with time.

152 Apart from the issue of insufficient studies on pollution source identification in rivers, most
153 of previous studies considered the location of the pollutant source to be known priori. This
154 assumption is not compatible with real-world condition, since in most cases the location of the
155 pollution source is also unknown as its intensity function. Introducing the source location as an
156 unknown, will have a significant effect on source identification process due to interaction
157 between a release at a variable source location and observational data. In other words, different
158 potential source location sets may result in significantly different solutions. Moreover, the
159 simultaneous identification of location and source release history is a very complicated ill-
160 posed problem, particularly in a case of multiple unknown pollution sources with time-varying
161 release pattern. The main motivations behind this study is to provide an innovative method for
162 simultaneous identification of the number, locations and release histories of multiple point
163 sources in a river network using minimum observational data and considering near real world
164 conditions namely unsteady and non-uniform flow as well as reactive pollutants. The proposed
165 method includes two main steps that are given below:
166 Step1: determining the number and suspected reaches to presence of sources by placement of
167 observation points in a specific manner and management of data collection at those stations.

Step 2: identification of exact location and intensity function of the source by solving the inverse source problem using a geostatistical approach.

The method is effective and easy to apply in complex river networks as well as single-branch ones. Moreover, it provides the possibility of simulators identification of all active pollutant sources. Hence the required computational time is significantly lower than common iterative methods such as simulation-optimization approach.

2. Material and Methods

2.1. Governing Equations and Statement of the problem

The main governing equation of solute transport in surface waters is advection-dispersion equation (ADE) (Taylor, 1954), which is a parabolic partial differential equation derived from a combination of continuity equation and Fick's first law. The one-dimensional ADE equation is as follows (Fischer et al., 1979):

$$\frac{\partial(AC)}{\partial t}+\frac{\partial(CQ)}{\partial x}-\frac{\partial}{\partial x}\left(AD\frac{\partial C}{\partial x}\right)+A\lambda C-\sum_{i=1}^{m}f_i(t)\,\delta(x-x_i)=0 \quad (1)$$

where, A is the flow area, C is the solute concentration, Q is the volumetric flow rate, D is the dispersion coefficient, λ is the first-order decay coefficient, m is the number of pollution sources, $f_i(t)$ is correspondent release history of ith pollution source, $\delta(x)$ is the Dirac delta function, x_i is the ith point source release location, t and x are the time and distance, respectively. It also should be mentioned that, hydrodynamic parameters (i.e., A, Q, D) in Equation (1) are obtained from the hydrodynamics model which is based on well-established Saint-Venant equations (Wu, 2007):

$$\frac{\partial A}{\partial t}+\frac{\partial Q}{\partial x}=0 \quad (2)$$

$$\frac{\partial Q}{\partial t}+\frac{\partial}{\partial x}\left(\frac{Q^2}{A}\right)+gA\frac{\partial z_s}{\partial x}+gAS_f=0 \quad (3)$$

in which z_s and S_f are water level and energy slope, respectively.

The general expression of the considered problem is that there are multiple pollutant point sources $S_1, S_2, \mathrm{K}, S_m$ in a river network, which the number, locations $(x_1, x_2, ..., x_m)$ and intensity functions $(f_1(t), f_2(t), ..., f_m(t))$ of those sources are unknown. The main objectives are to present a methodology for simultaneous identification of these sources characteristics (i.e. their number, locations, and intensity functions), and obtaining a unique response for the considered inverse source problem with a minimum measured concentration data at observation points. The proposed method consists of two main steps. The method starts with the determination of a spatial range in which the source of pollution is likely to be present. Then the location and approximate release history of pollution sources are recovered by means of a geostatistical approach, that considered simultaneously all the possible candidates. The method is effective and easy to apply in complex river networks as well as single-branch ones. Moreover, since in each simulation all active pollutant sources are identified, the required computational time is significantly lower than common iterative methods such as simulation-optimization approach. More details are given in following sections.

2.2. Step1: Determination of the Number and Approximate Location of Pollution Sources

In order to determine the approximate location of pollutant sources, some observation points are considered with a specific arrangement and data collection at those observation points are managed based on specified condition of each problem. In order to provide the concentration data and proceed with the identification process, two types of observation points are defined, main $(M_1, M_2, ..., M_n)$ and secondary stations $(P_1, P_2, ..., P_k)$ (Figure 1). The main stations collect concentration-time data continuously, but the secondary ones collect data occasionally and on-demand. The placement of main and secondary stations is based on some priori information including desired activity time for retrieval and accuracy of spatial range for

pollution source localization. The main stations are placed in a way that the travel time between two successive main stations always is less than or equal to the expected activity time for the sources. The travel time between successive main stations for each branch of the river network and is calculated using following equation (Chapra, 2008):

$$\bar{T} = \frac{\sum_{i=1}^{n-1} \left(C_i t_i + C_{i+1} t_{i+1} \right) \left(t_{i+1} - t_i \right)}{\sum_{i=1}^{n-1} \left(C_i + C_{i+1} \right) \left(t_{i+1} - t_i \right)} \tag{4}$$

in which $\bar{T}$ is travel time, C_i is the concentration at temporal instant t_i. The secondary stations are arranged in a way that the distance between two successive stations be equal to the accuracy which expected for approximate location of the sources. This configuration of monitoring station makes it possible to identify all active pollutant sources with minimum measurement data and avoid additional data collection as well as related costs.

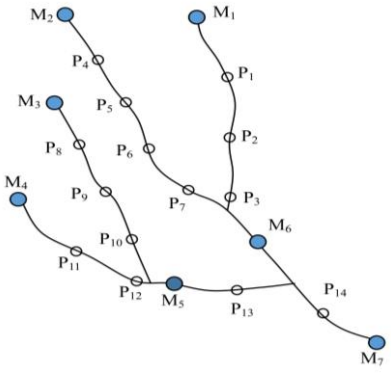

Figure 1- A hypothetical river network and arrangement of main and secondary stations

The key step in the algorithm is comparison of observed and simulated concentration data in the main stations, so that any difference between these two sets of data is a sign of existence of a pollutant source at the upstream of that particular station. The simulated data are taken from an integrated flow and transport model, which solves equation (1) - (3) in a river network for a case of no active pollutant source. It is a real-time simulation model which continuously

227 executed and its outputs namely concentration-time data $C(x,t)$ are used in solving the inverse
228 source problem by proposed algorithm.

229 Once a main station detects a difference between observed and simulated concentration
230 data, depending on the type of communication topology of monitoring system a command will
231 be send from a control center or directly from that main station to all secondary stations which
232 have been located between that main station and the first main station at upstream of it, to
233 collect a concentration data at the instant of difference detection. The first secondary station
234 from upstream which shows a difference between observed and simulated data, guide us to the
235 approximate location of the source. In other words, the pollution source must be located in the
236 reach between that secondary station and the first secondary station at its upstream (Figure 2).
237 After determining the approximate location of the pollution source, following actions should
238 be done:

239 1. The secondary station which detected the difference as well as the secondary station
240 located at upstream of that, should start to continuous data collecting, to assure that
241 other active sources at the upstream and/or downstream of that suspected reach, will be
242 detected as well,
243 2. The source location should be determined more accurately, to proceed to find the
244 intensity function of detected source,
245 3. The forward model should be revised to include the characteristics of the identified
246 source.

247 It also should be noted that the continuous data collecting at secondary stations, which frame
248 the source location, will be stopped after the full passage of pollution cloud from secondary
249 station that located at the downstream bound of suspected reach. The identification process of
250 approximate location of a case with multiple pollutant sources, are quite similar to what was
251 described for the case with one active source (Figure 3).

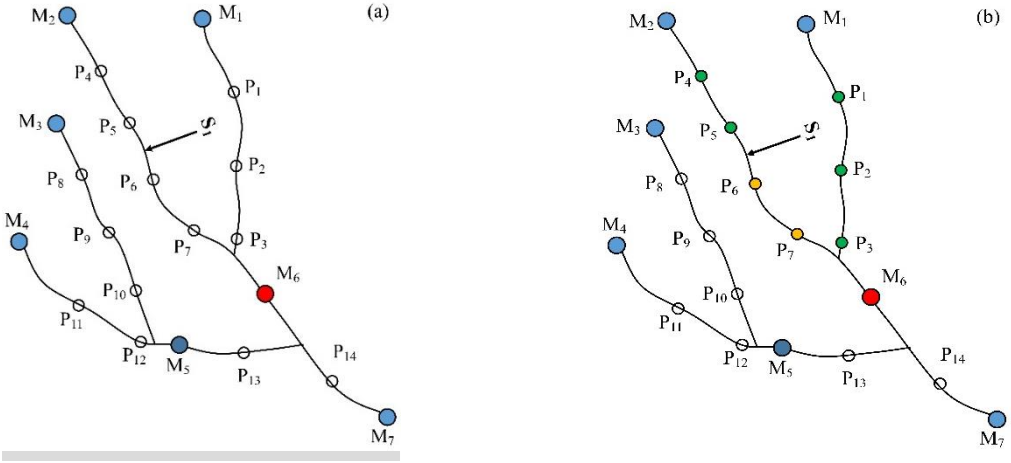

252 **Figure 2-** detection of approximate location in the case of one active source

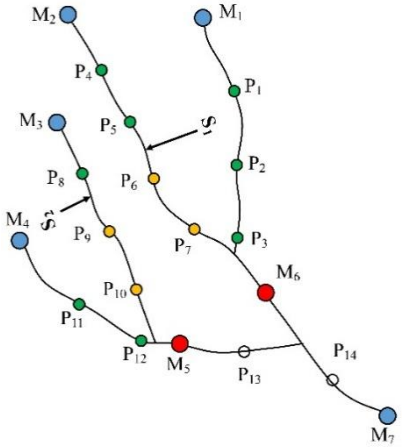

253 **Figure 3**- A case with two active sources

254 2.3. Step 2: Recovering the Characteristics of Pollutant Sources by
255 Means of a Geostatistical Method

256 After determining the number and suspected reaches to presence of pollution sources, the exact
257 location and approximate intensity function of pollution sources should be determined. Hence,
258 at first the mentioned reaches are divided to some sub-reaches and the potential location of
259 pollutant sources are considered at the center of those sub-reaches. Then, by solving an inverse
260 source problem, the true location of the pollutant sources (i.e., where the pollutant injection has
261 most likely originated) is determined as a location that the highest contaminant release history
262 is obtained. In order to solve the inverse source problem a Geostatistical method (GS) has been
263 used in this study. Regarding the linearity of equation (1) the solution of these equation subject

to initial and boundary conditions (i.e., $C(x,0)=C_0(x), C(0,t)=C_{in}(t), C(L,t)=0$) is (Skaggs and Kabala, 1994):

$$C(\mathbf{x},t)=\int_0^t f(\tau)K(\mathbf{x},t-\tau)d\tau \tag{5}$$

where $K(\mathbf{x},t-\tau)$ is the transfer function (TF), that describes the effect in time at a certain location x by a unitary impulse source which is released at x_0 and time τ. If *M* observational data be available and the time domain is discretized in *N* instants, a general expression of the relation between the observations and the source can be written as follows:

$$\mathbf{z}=\mathbf{h}(\mathbf{f})+\mathbf{v} \tag{6}$$

where $\mathbf{z}$ is a $[M\times 1]$ random vector of observations, $\mathbf{f}$ is a $[N\times 1]$ random vector of discretized release history, $\mathbf{h}$ is the model function and $\mathbf{v}$ is a $[M\times 1]$ random vector that represents the measurement errors. The error vector $\mathbf{v}$ is Gaussian with a zero mean and a covariance matrix as $\mathrm{R}=\sigma_R^2\mathrm{I}$ in which $\mathbf{I}$ is the $[M\times M]$ identity matrix. It also should be noted that N ? M, which means that there are more unknowns than measurements. By comparing equation (6) and (5) it can be concluded that the function $\mathbf{h}(\mathbf{f})$ is linear and therefore equation (6) can be rewritten as follows:

$$\mathbf{z}=\mathbf{H}\mathbf{f}+\mathbf{v} \tag{7}$$

where $\mathbf{H}$ is a $[M\times N]$ matrix known as transfer matrix and its generic element is:

$$H_{i,j}=\Delta\tau\begin{cases}K(t_i-\tau_j) & t_i>\tau_j\\ 0 & t_i<\tau_j\end{cases} \tag{8}$$

in which $\Delta\tau$ is time step between two successive discretization of intensity function, t_i and τ_j are observation instants and release time, respectively.

The $H_{i,j}$ element of transfer matrix represents the effect of a release at τ_j on observation data z_i at which collected at t_i. As shown in equation (8), to construct the $\mathbf{H}$ matrix, it is necessary to calculate TFs at different time instants. TFs describe the response of the system

to a unit impulse injection. Therefore, to calculate them, the ADE equation (equation (1)) need to be solved for a unitary release function at the source location and for different time instants. In case of simple problems with steady flow, regular cross-sections and constant parameters, TFs can be determined using analytical procedures. However, in many practical applications, with unsteady flow, irregular cross-sections and variable parameters using analytical formulas in evaluation of TFs values, is only possible by considering a series of simplifying assumptions. As a consequence, a rough approximation in the solution of inverse problem expected, that is not desirable. Due to the complex conditions that considered in this study, the transfer functions have been calculated using the finite volume numerical method. To calculate the value of $H_{i,j}$ terms, several runs of the numerical model were performed. In case of unsteady flow, the numerical model has to be performed for all the τ_j instants that are desired to recover the intensity function, i.e., *N* times. For each run the unit release is modelled as Dirac delta function $\delta(\tau_j)$ at potential source location and breakthrough curves at observation points were calculated. In other words:

$$H_{ij} = C(x,t_i) = \int_0^{t_i} \delta(\tau_j) K(x,t_i - \tau_j)\, d\tau \tag{9}$$

The equation (7) is a system of ill-posed equations that cannot be solved by conventional methods. In order to overcome this difficulty, it is assumed that **f** has a normal distribution with mean and covariance as follows:

$$E[\mathbf{f}] = \mathbf{X}\beta \tag{10}$$

$$E\left[(\mathbf{f} - \mathbf{X}\beta)(\mathbf{f} - \mathbf{X}\beta)^T\right] = \mathbf{Q}(\boldsymbol{\theta}) \tag{11}$$

where **X** is a $[N \times 1]$ unit vector, β is the unknown mean, $\boldsymbol{\theta}$ is a vector of unknown structural parameters of the covariance function, and **Q** is the covariance matrix of the release $f(\tau)$. In this research, a Gaussian covariance matrix has been considered, whose formulation is as follows:

$$\mathbf{Q}\left(\tau_i-\tau_j\left|\boldsymbol{\theta}\right.\right)=\sigma^2\, exp\left[-\frac{\left(\tau_i-\tau_j\right)^2}{I_f{}^2}\right] \tag{12}$$

where $\theta^T=\left[\sigma^2, I_f\right]$ are structural parameters.

The reconstruction of pollutant source intensity function in the geostatistical method consist of two steps. In the first step, known as structural analysis, the structural parameters of the covariance function θ are determined, and in the second step, the contaminant source intensity function (**f**) is estimated using the kriging method. Structural parameters are determined by minimizing the following objective function (Snodgrass and Kitanidis, 1997):

$$L\left(\boldsymbol{\theta}\right)=-\ln\left[\, p\left(\mathbf{z}\left|\boldsymbol{\theta}\right.\right)\right]\propto\frac{1}{2}\ln\left(\left|\Sigma\right|.\left|\mathbf{X}^T\mathbf{H}^T\Sigma^{-1}\mathbf{H}\mathbf{X}\right|\right)+\frac{1}{2}\mathbf{z}^T\Xi\,\mathbf{z} \tag{13}$$

in which:

$$\Sigma=\mathbf{H}\mathbf{Q}\mathbf{H}^T+\mathbf{R} \tag{14}$$

$$\Xi=\Sigma^{-1}-\Sigma^{-1}\mathbf{H}\mathbf{X}\left(\mathbf{X}^T\mathbf{H}^T\Sigma^{-1}\mathbf{H}\mathbf{X}\right)^{-1}\mathbf{X}^T\mathbf{H}^T\Sigma^{-1} \tag{15}$$

the minimization of Equation (13) is a well-posed problem, since the number of observation **z** is greater than the number of structural parameters $\boldsymbol{\theta}$. In equations (14) and (15), **R** is the covariance matrix of error in the observational data (**v**). It should be noticed that the value of the unknown mean β is not relevant as it does not appear in the Equations (13-(15). The β coefficients are eliminated from Equation (13) by averaging over all possible values of it (Hoeksema and Kitanidis, 1985, Kitanidis, 1995).

Once the structural parameters $\boldsymbol{\theta}$ are calculated, the intensity function is estimated through a kriging system (De Marsily, 1986):

$$\hat{\mathbf{f}}=\boldsymbol{\Lambda}\mathbf{z} \tag{16}$$

Equation (16) is a linear estimator. It is unbiased and minimizes the estimate error variance (Boano et al., 2005, Butera et al., 2013), in other words:

$$E\left[\hat{\mathbf{f}}-\mathbf{f}\right]=0 \tag{17}$$

$$\min_{\hat{\mathbf{f}}} E\left[\left(\hat{\mathbf{f}}-\mathbf{f}\right)-\left(\hat{\mathbf{f}}-\mathbf{f}\right)^T\right]. \tag{18}$$

$\mathbf{\Lambda}$ is a $[N \times M]$ matrix of Kriging weights that obtained from solving the following system of equation:

$$\begin{bmatrix} \mathbf{\Sigma} & \mathbf{HX} \\ (\mathbf{HX})^T & 0 \end{bmatrix} \begin{bmatrix} \mathbf{\Lambda}^T \\ \mathbf{M} \end{bmatrix} = \begin{bmatrix} \mathbf{HQ} \\ \mathbf{X}^T \end{bmatrix} \tag{19}$$

where M is a $[1 \times N]$ matrix of Lagrange multipliers (De Marsily, 1986). The mean of the release history is then estimated by equation (16), while its covariance matrix $\mathbf{V}$ can be evaluated as:

$$\mathbf{V} = -\mathbf{XM} + \mathbf{Q} - \mathbf{QH}^T \mathbf{\Lambda}^T \tag{20}$$

Using Equation (20) the confidence interval of 95% can also be determined, so that for every instant of time t_i, the confidence interval can be calculated as $\hat{f}_i \pm 2\sqrt{V_{ii}}$ in which V_{ii} is the estimation error variance of $\hat{f}_i$.

The GS method is a practical and efficient method, but sometimes it obtains non-physical results, including negative concentrations. Usually, this problem is alleviated by introducing additional constraints to the unknown variable (Box and Cox, 1964, Snodgrass and Kitanidis, 1997, Michalak and Kitanidis, 2003, 2004a). This constrain is imposed by using a power transformation of the unknown variables. The new unknown function is written as follows:

$$\tilde{\mathbf{f}} = \alpha\left(\mathbf{f}^{1/\alpha} - 1\right) \tag{21}$$

where α is a small positive parameter, the value of which is chosen in a way that ensure $\tilde{\mathbf{f}} > -\alpha$. Kitanidis and Shen (1996) presented a method for choosing the optimal value of parameter α.

Then, the transformed variable $\tilde{\mathbf{f}}$ should be substituted to original variable f in equation (6), so equation (6) is replaced by the following one:

$$\mathbf{z} = \tilde{\mathbf{h}}(\tilde{\mathbf{f}}) + \mathbf{v} \tag{22}$$

in which:

$$\tilde{\mathbf{h}}(\tilde{\mathbf{f}}) = \mathbf{h}\left[\left(\left(\tilde{\mathbf{f}} + \alpha\right)/\alpha\right)^{\alpha}\right] \tag{23}$$

since the model is no longer linear with respect to the transformed variable $\mathbf{f}^{\alpha}$, the solution must be evaluated using successive iterations. More details could be found in Kitanidis (1995). The method can easily be extended to the case of *m* multiple independent point sources located at $\mathrm{x}=\left[x_1, x_2, \mathrm{K}, x_m\right]$ and p distinct measurement points located at $\mathrm{x}_{obs}=\left[x_1, x_2, \mathrm{K}, x_p\right]$. Regarding to the linearity of the ADE with respect to the concentration C (x, t), it can be written:

$$C(x_{obs}, t)=\sum_{j=1}^{m} f_j(\tau) K\left(x_{obs_i}-x_j, t-\tau\right)\Delta\tau \tag{24}$$

In which)24(is the number of observation points. The matrix form of equation i=1,2,…,p is as follows:

$$\mathbf{z}=\mathbf{H}\mathbf{f}+\mathbf{v} \tag{25}$$

where:

$$\mathbf{z}^T=\left[\mathbf{z}_1\ \mathbf{z}_2 \mathrm{K}\ \mathbf{z}_P\right] \tag{26}$$

$$\mathbf{f}^T=\left[\mathbf{f}_1\ \mathbf{f}_2 \mathrm{K}\ \mathbf{f}_m\right] \tag{27}$$

$$\mathbf{H}=\begin{bmatrix} \mathbf{H}_{11} & \mathrm{L} & \mathbf{H}_{1m} \\ \mathrm{M} & \mathrm{O} & \mathrm{M} \\ \mathbf{H}_{i1} & \mathrm{L} & \mathbf{H}_{pm} \end{bmatrix} \tag{28}$$

Equation (25) is a system of equation in which, H_{ij}, i=1,2,…,p , j=1,2,…,m , is the transfer matrix corresponding with the effect of the pollutant source release at x_i on the measured concentration data at x_j. Since pollutant sources are independent, the covariance matrix is a block matrix as follows:

$$\mathbf{Q}=\begin{bmatrix} \mathbf{Q}_1 & \mathrm{L} & 0 & 0 \\ 0 & \mathbf{Q}_2 & \mathrm{L} & 0 \\ \mathrm{M} & \mathrm{M} & \mathrm{O} & \mathrm{M} \\ 0 & 0 & \mathrm{K} & \mathbf{Q}_m \end{bmatrix} \tag{29}$$

The rest of steps for solving the system of equations (22) are similar to solving for a single pollutant source, described in the previous sections. Figure 4 represents a flowchart of overall identification process.

3. Results and Discussion

In this section an application of the proposed method for simultaneous identification of pollution source characteristics in a river network is presented. For this purpose, a hypothetical river network consisting of a main stream (B1) and two tributaries (B2 and B3) with unsteady flow conditions and irregular cross-sections has been considered. The general outline of the considered river network along with the arrangement of main and secondary stations is shown in Figure 5. The main and secondary stations were placed based on the criteria mentioned in section 2.2. First, by assuming the activity duration of 10 hours and more for retrieval and based on the calculated travel time from Equation (4), the location of main stations in all branches, was determined. After that, based on the desired accuracy for spatial range, secondary stations were located in the intervals of 8, 7 and 9 km for the main, second and third branches, respectively.

A complete list of main and secondary stations of each branch, along with its distance from the upstream and the travel time between two successive main stations, is given in Table 1. It can been seen from Table 1 that the travel time between two successive main stations is always less than or equal to the expected activity time for retrieval (10 hours). It also should be mentioned that main stations which located at the beginning of branches, namely M1, M5 and M7, are only used to record upstream boundary conditions of the forward flow and transport model and are not used in the identification process.

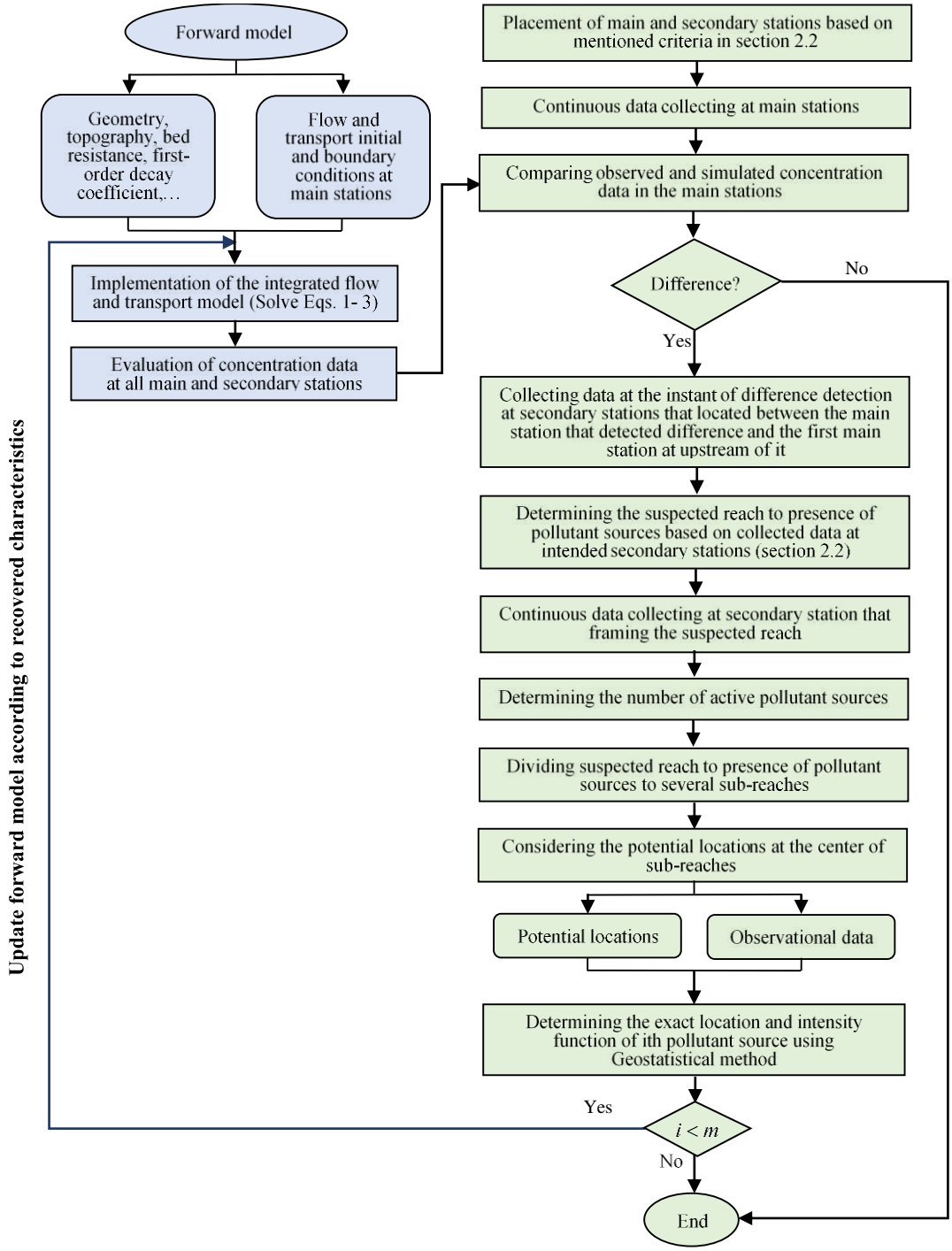

375

376 **Figure 4-** Flowchart of identification process

377 After placement of main and secondary stations, in order to calculate the spatial and
378 temporal distribution of pollutant concentration in all stations, the forward flow and transport
379 model are performed twice with give boundary condition (Figure 6). First without considering
380 pollutant sources and then with considering them. The first set of results are used as simulated
381 data and the second ones are used as observed data. In order to evaluate the performance of

382 proposed method three different scenarios in terms of number, release location and activity
383 duration has been considered. The main characteristics of those scenarios were listed in Table
384 2. Complementary explanations for each scenario are given below.

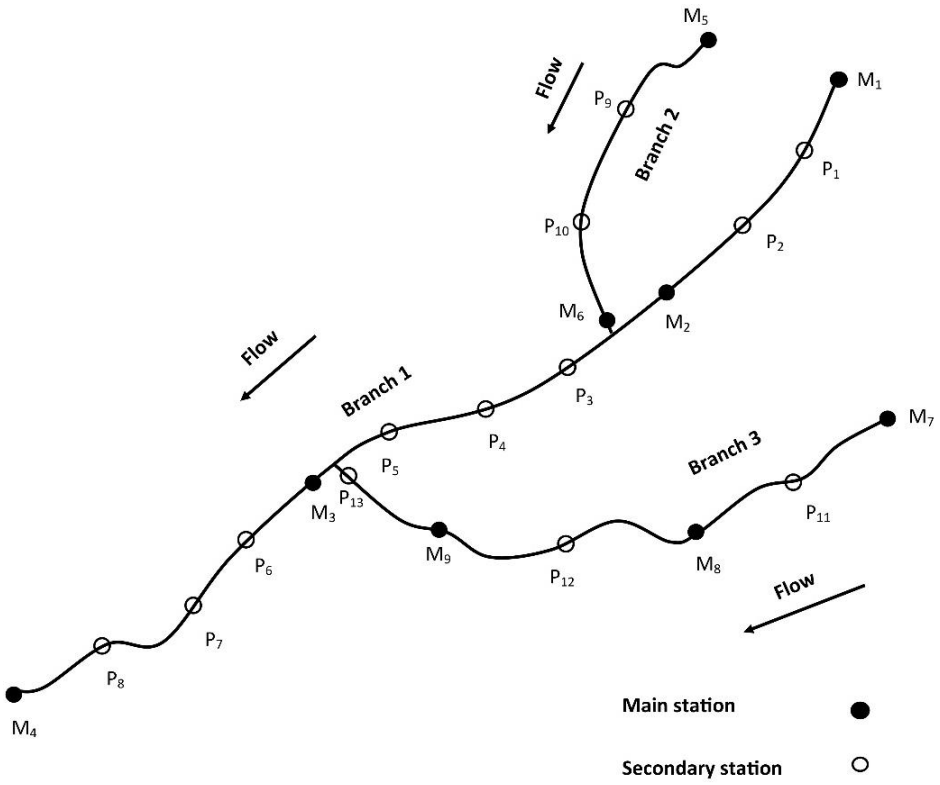

385 **Figure 5**- The schematic of hypothetical river network along with the arrangement of the main and
386 secondary stations

387 **Table 1**- Monitoring stations

First Branch (B1)												
station	M_1	P_1	P_2	M2	P_3	P_4	P_5	M_3	P_6	P_7	P_8	M_4
Distance from upstream (km)	0	8	16	24	32	40	48	57	65	73	81	90
Travel time (hr.)	10					9.95				9.82		
Second Branch (B2)												
station	M_5			P_9			P_{10}			M_6		
Distance from upstream (km)	0			7			14			21		
Travel time (hr.)	9.85											
Third Branch (B3)												
station	M_7		P_{11}		M_8		P_{12}		M_9		P_{13}	
Distance from upstream (km)	0		9		18		27		36		45	
Travel time (hr.)	9.98						10				6.12	

388

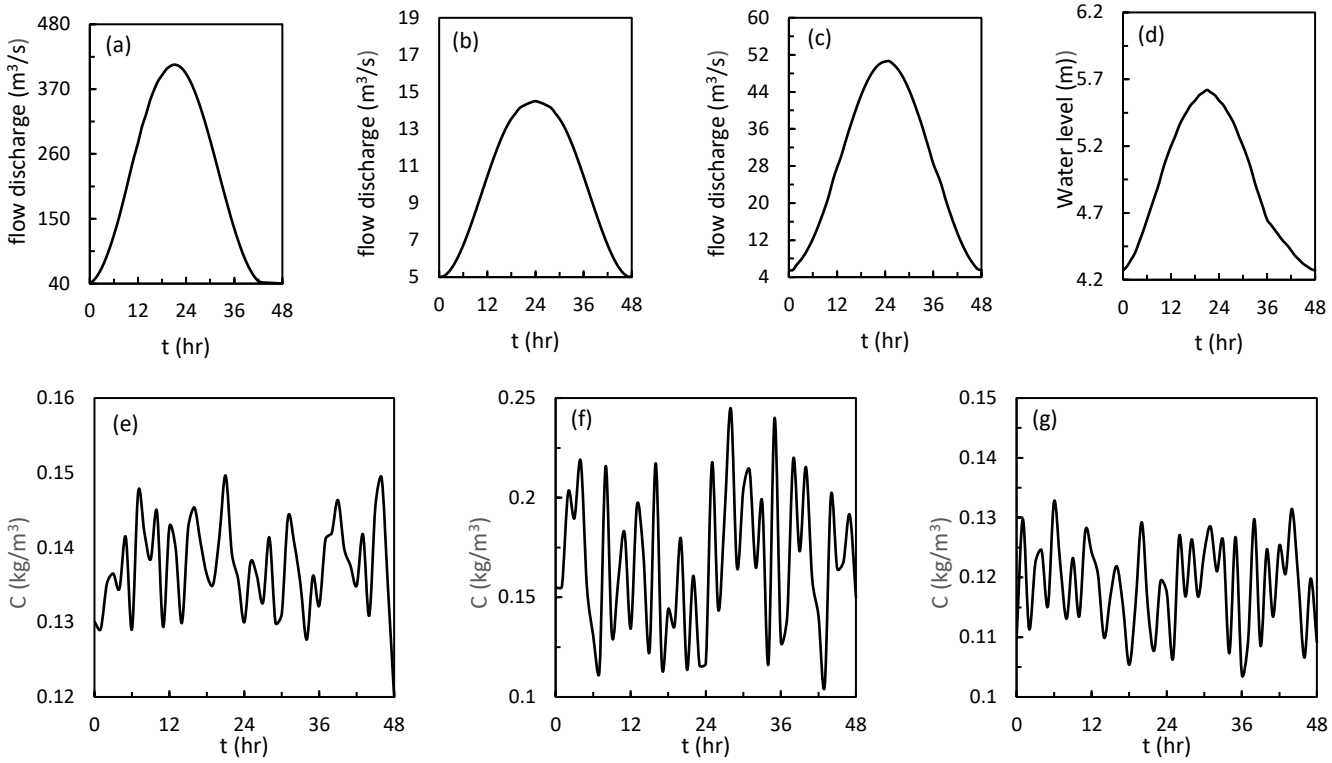

Figure 6- Flow and transport boundary conditions, (a)-(c) upstream boundary conditions of flow model at M1, M5 and M7, respectively, (d) upstream boundary conditions of flow model at M4 and (e)-(g) upstream boundary conditions of transport model at M1, M5 and M7, respectively.

Table 2- The main characteristics of different considered scenarios

Scenario	Number of Active Sources	Release location (Branch/Distance from Upstream)	Activity Duration (hr.)	Simultaneous Active Sources
1	1	B2-8.75	11	-
2	2	B2-8.75	11	No
		B1-46	16	
3- Test 1	3	B2-8.75	11	Yes
		B1-46	16	
		B1-10	13.5	
3-Test 2	3	B2-8.75	11	Yes
		B1-10	13.5	
		B1-46	16	

3.1. Scenario 1: one active source

In this example, it is assumed that there is only one active pollution source at 8.75 km of the upstream end of the second branch (B2) with activity duration of 11 hours (Figure 7). As mentioned in Section 2.2, it is necessary to first determine the suspected reach to presence of the source by comparing the observed and simulated concentration data at all main stations. Figure 8 shows a comparison of observed and simulated concentration data at main stations for this example. It should be noted that the initial period with zero concentration is due to the

initial condition that was chosen for the sake of simplicity, and it does not affect the results in other ways. It can be seen from Figure 8 that the first main station which recorded the difference between the observed and simulated concentration data is M6, located at 21 km of the upstream end of the second branch of the hypothetical river network.

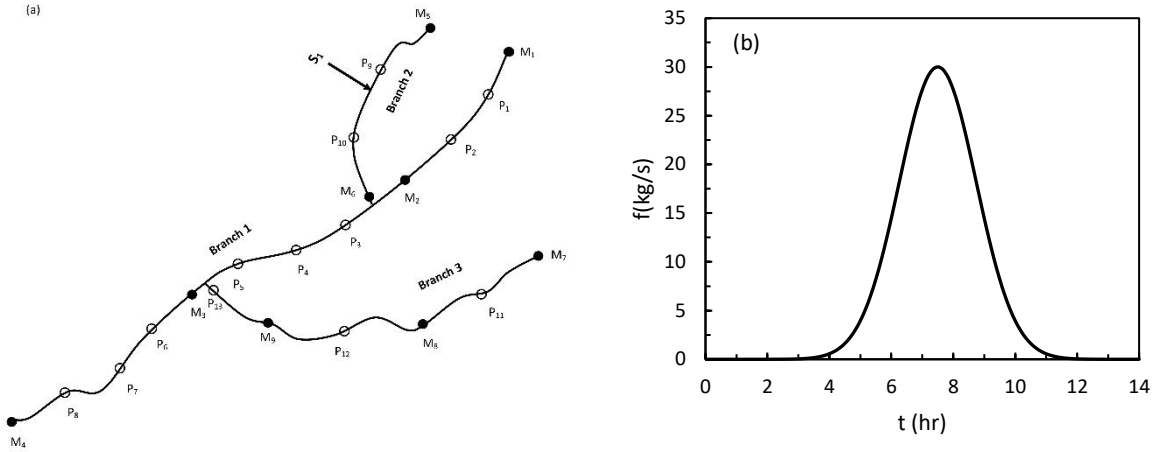

Figure 7- (a) location and (b) intensity function of pollutant source (scenario 1)

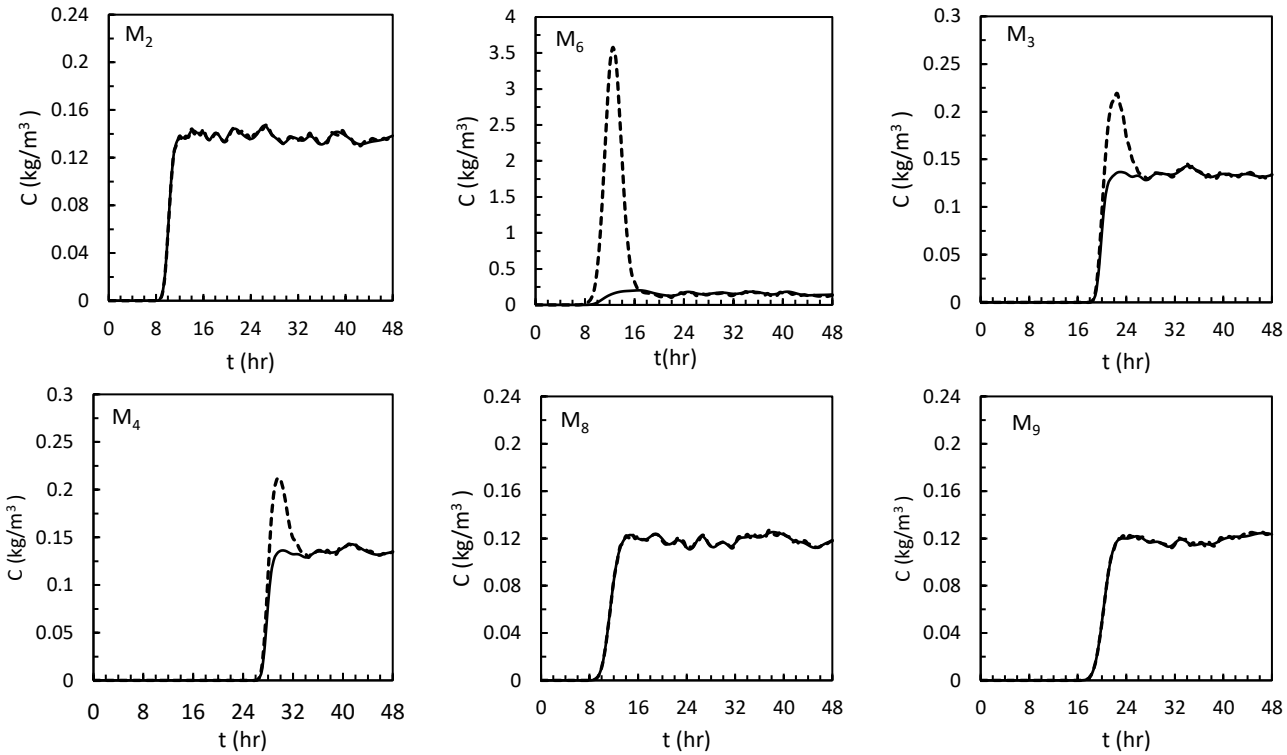

Figure 8- Comparison of simulated and observed data in main stations (scenario 1) (solid line: simulated and dashed line: observed data)

After detection the difference in data at M6, a concentration observation data should be collected at all secondary stations that located at upstream of M6 (namely, P9 and P10) at the instant of difference detection. Figure 9 shows the collected data at these secondary stations

and their comparison with the simulated data. As it can be seen from Figure 9, there is a significant difference between the observed and simulated concentration data at P10, while the observed and simulated data at P9 are exactly the same. Therefore, it can be concluded that the release point of the pollutant source is in the reach between P9 and P10, i.e. at the range of 7 to 14 km of the upstream end of the B2.

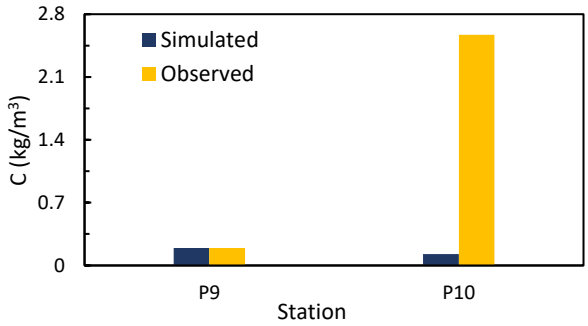

Figure 9- Comparison of simulated and observed data in secondary stations at the instant of difference detection between the simulated and observed data in M6 (scenario 1)

Subsequently, secondary stations that located at the upstream and downstream of suspected reach, should begin to permanent data collection to ensure that there is no other active source. Figure 10 shows a comparison of observed and simulated data at P9 and P10. As it can be seen from Figure 10, there is no difference between the observed and simulated data at P9, which means that there is no active source at the upstream of suspected reach, during the period of activity of the discovered source. Comparison of these two series of data in P10 shows the difference. According to the general form and peak concentration of observed concentration-time curve and comparing it with the concentration-time curve at M6 (Figure 8), it can be deduced that this difference caused by the source that just has been discovered and there are no other active sources.

In the next step, the suspected reach to presence of pollutant source (i.e., 7 to 14 km of the upstream end of the B2) is divided into two sub-reaches (namely from 7 to 10.5 km and 10.5 to 14 km) and the potential locations of the pollutant source are considered at the center of these sub-reaches (i.e., 8.75 and 12.25 km of the upstream end of the B2). Then, by implementing the inverse model and using the spatial distribution of concentration data at all

stations located downstream of suspected reach and at the instant of full passage of pollution cloud from P10, exact location and approximate intensity function of pollutant source are determined. Figure 11 shows the exact and recovered intensity function of the pollutant source with 95 percent confidence interval for both potential locations. As it can be seen from the Figure 11, for the case where the potential location is equal to the exact location of the assumed pollutant source (i.e. 8.75 km of the upstream end of the B2), there is a good match between the exact and recovered intensity function. While, in the case where the potential location is considered at 12.25 km of the upstream end of the B2, a close to zero amount for intensity function has been obtained.

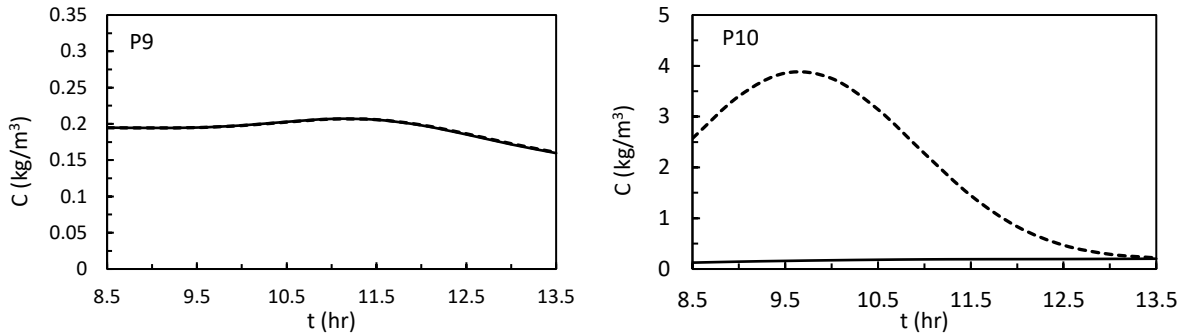

Figure 10- Comparison of observed and simulated data in secondary stations located at the upstream and downstream of suspected reach during the period of permanent data collection by those stations (scenario 1) (solid line: simulated and dashed line: observed data)

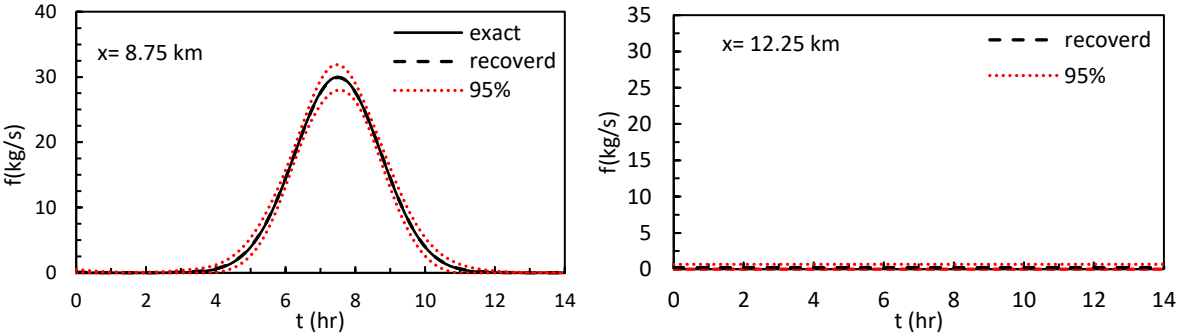

Figure 11- Recovered intensity function at two potential locations using observed data at all main and secondary stations that located downstream of the suspected reach (scenario 1)

After determining the exact location of the source, it is necessary to identify its intensity function more accurately, assuming that the source location is known. So, the intensity function is recovered using observed time-concentration data at the first main station at downstream (M6). The results are shown in Figure 12. The error indices for both approximate recovery

using the spatial distribution of concentration data and the exact recovery using time-concentration data are given in Table 3. It should be mentioned that, the indices that used to evaluate the performance of proposed method include square of correlation coefficient (R^2), root mean square error (RMSE), mean absolute error (MAE) and Euclidean distance (de). The last one, indicates the distance between the upper (σu) and lower (σl) bound of the 95% confidence interval and it is used to evaluate the uncertainty of recovered release history based on the observation data (Equation (30))

$$de = \sqrt{\sum_{i=1}^{n} \left(\sigma u_i - \sigma l_i\right)^2} \tag{30}$$

Figure 12 and the error indices in Table 3 indicate that in both cases the proposed model has been retrieved the intensity function with almost a same accuracy. The only difference is concerned with the width of 95% confidence interval, which is wider in the case of retrieval using spatial distribution of concentration data. This means that there are more release histories that consistent with the observations. This is also an indication of the increased uncertainty in estimations. The main reason for this results is sparsity of spatial distribution of concentration data compared to time-concentration data, which makes the ill-posedness issue more sever and causes more uncertainty in identification process.

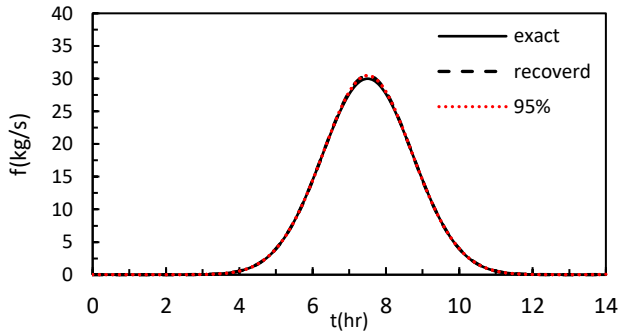

Figure 12- Recovered intensity function by considering the exact location of the source and using observed concentration-time data at the first main station at downstream (M6)

471 **Table 3**- Error indices of scenario 1

Index	Recovery using spatial distribution of concentration data	Recovery using observed concentration-time data at the first main station at downstream (M6)
R^2 (%)	99.99	99.99
RMSE (kg/s)	0.05	0.04
MAE (kg/s)	0.045	0.027
de (kg/s)	9.12	0.24

472 ## 3.2. Scenario 2: two asynchronous active sources

473 In this example, it was assumed that there are two active pollutant sources in the river network
474 during the simulation time, so that the start time of activity of the second source is after the end
475 of activity of the first pollutant source. The first source was considered similar to the scenario
476 one, at 8.75 km of the upstream end of the B2 and the second source assumed at 46 km of the
477 upstream end of the B1 (Figure 13). After identification of the first source, similar to the
478 scenario 1, the forward model is modified considering the identified location and release
479 history of the first source. After revising the forward model, a comparison of the observed and
480 simulated data at the main stations (Figure 14) shows that a difference between these series of
481 data at the M3 located at 57 km of the upstream end of the B1. This indicates the presence of
482 an active source at the upstream of that station. So, it is necessary to collect a concentration
483 data at the instant of recording the difference at all secondary stations located between station
484 M3 and the first main stations upstream (i.e. M2, M6 and M8). Figure 15 depicts the collected
485 data at these secondary stations and their comparison with the simulated data. As can be seen
486 from Figure 15 the only secondary station that recorded the difference between the observed
487 and simulated data is the P5 , located 48 km of the upstream end of the B1.Hence, it can be
488 said that the suspected reach to presence the second source is between P5 and the upstream
489 secondary station (P4).

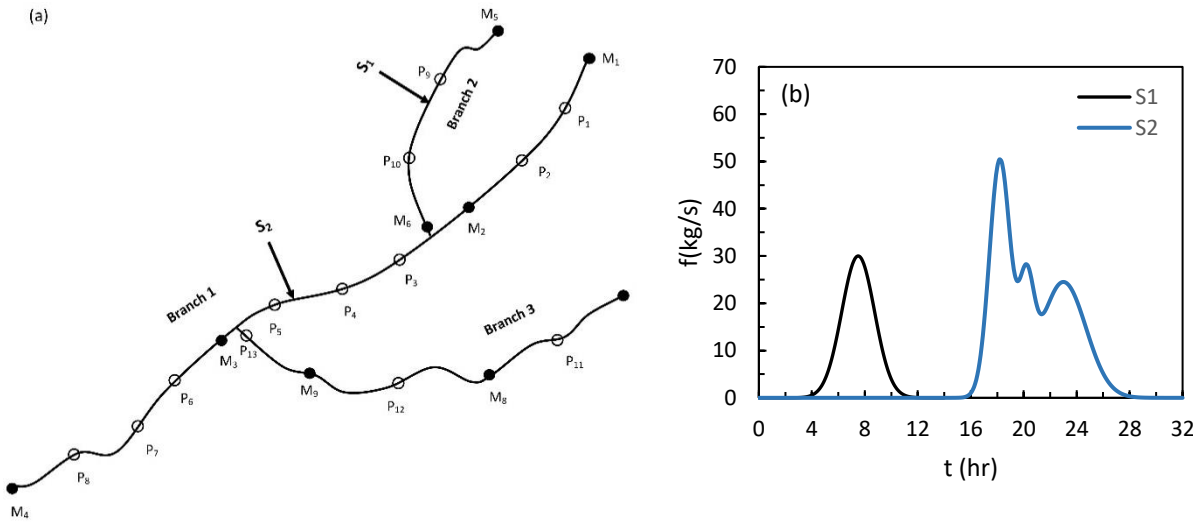

490 **Figure 13**- (a) location and (b) intensity function of pollutant sources (scenario 2)

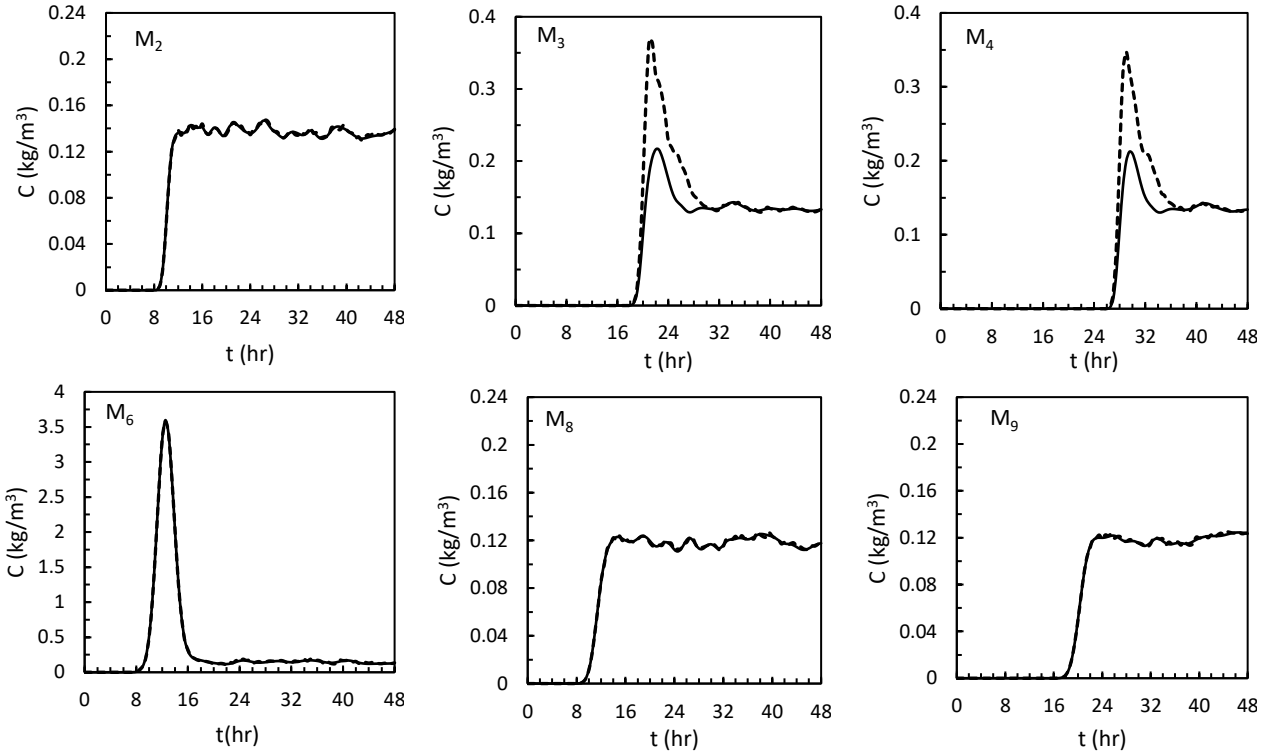

491 **Figure 14**- Comparison of simulated and observed data in main stations (scenario 2) (solid line:
492 simulated and dashed line: observed data)

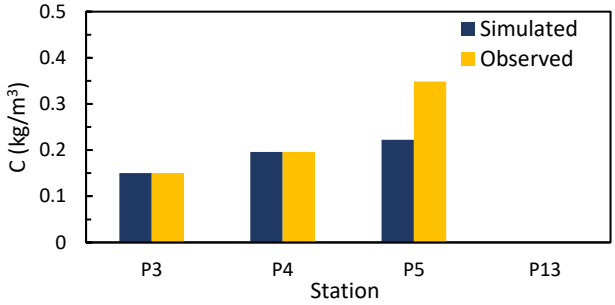

493 **Figure 15**- Comparison of simulated and observed data in secondary stations at the instant of
494 difference detection between the simulated and observed data in M3 (scenario 2)

Subsequently, secondary stations that are located immediately upstream and downstream of suspected reach, should begin to permanent data collection to ensure that there is no other active source. A comparison of observed and simulated data at P4 and P5 are shown in Figure 16. As can be seen from Figure 16, there is no difference between the observed and simulated data at P4, which means there is no active source at the upstream during the activity time of the discovered source. A comparison of these two sets of data in the P5 represents a difference. By comparing the general form and peak concentration of observed concentration-time curve and concentration-time curve at M3 (Figure 14), it can be concluded that this difference is due to the discovered source and there are no other active pollutant sources.

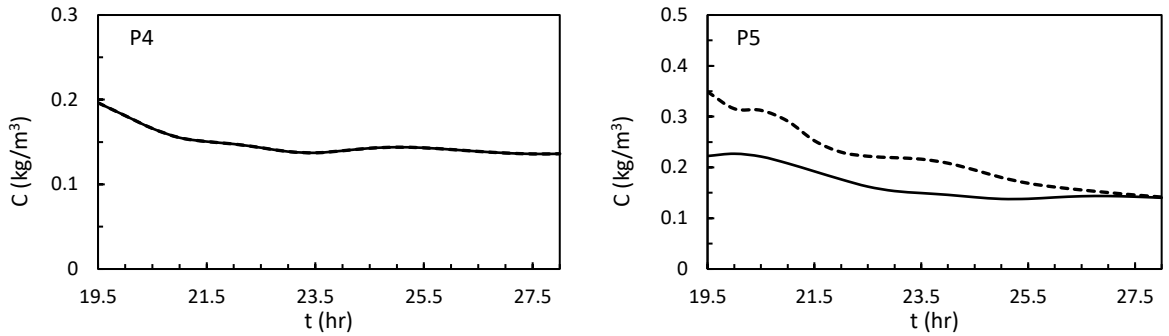

Figure 16- Comparison of observed and simulated data in secondary stations located at the upstream and downstream of suspected reach during the period of permanent data collection by those stations (scenario 2) (solid line: simulated and dashed line: observed data)

In the next step, the suspected reach is divided into two sub-reaches with equal length and the potential locations of the source are considered in the center of each of these sub-reaches, namely 42 and 46 km of the upstream end of the B1. Then, the exact location of S2 and its approximate intensity function are determined by implementing inverse model and using the spatial distribution of concentration data in all stations located at the downstream of suspected reach. The results are presented in Figure 17. According to these results, it can be concluded that the second source is located 46 km of the upstream end of the B1, which is corresponded to the assumed location.

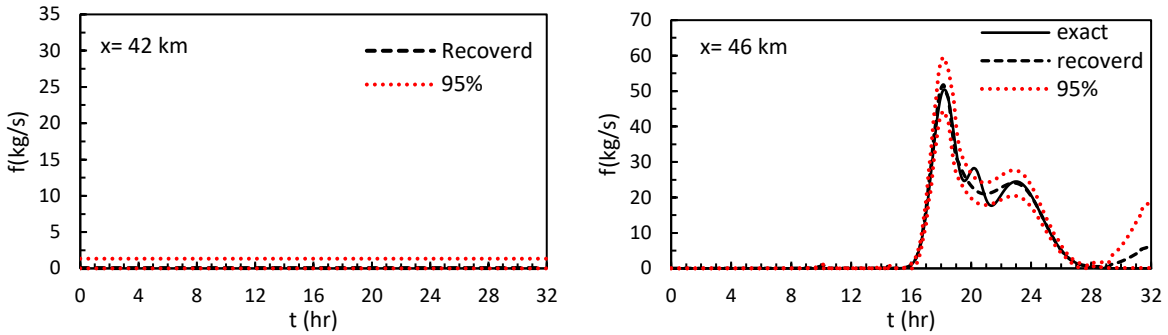

Figure 17- Recovered intensity function at two potential locations using observed data at all main and secondary stations that located downstream of the suspected reach (scenario 2)

Finally, by assuming the known source location and using concentration-time data at M3, the intensity function is determined more accurately. The results are shown in Figure 18. The error indices for both approximate recovery using the spatial distribution of concentration data and the exact recovery using time-concentration data are given in Table 4. Figure 18 and the error indices in Table 4, suggested that the accuracy of the results obtained using the concentration-time data is slightly better than the accuracy of the results obtained using the spatial distribution of concentration data. In addition, the 95% confidence interval opening is wider at the case of recovery with spatial distribution of concentration data, which is interpreted as more uncertainty in results. Given that the spatial distribution of concentration data are usually sparse and the number of available data is much less than the desired temporal instants for retrieval of intensity function, the existence of a higher degree of uncertainty in the results is inevitable.

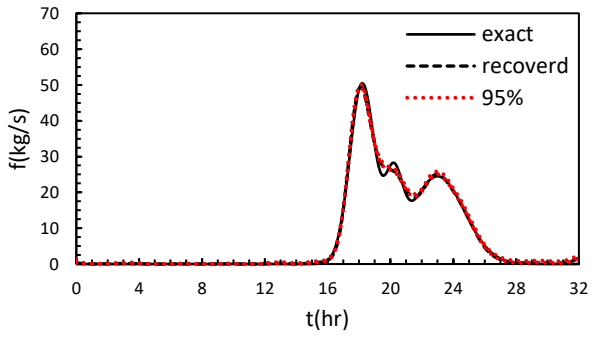

Figure 18- Recovered intensity function by considering the exact location of the source and using observed concentration-time data at the first main station at downstream (M3)

533 **Table 4-** Error indices of scenario 2

Index	Recovery using spatial distribution of concentration data	Recovery using observed concentration-time data at the first main station at downstream (M3)
R^2 (%)	98.32	99.68
RMSE (kg/s)	1.64	0.6975
MAE (kg/s)	0.7996	0.3823
de (kg/s)	81.2366	15.2694

534 ## 3.3. Scenario 3: three active sources, with at least two simultaneously active

535 ## sources

536 In order to show the capabilities of the proposed model in the case where several sources are
537 simultaneously active, this example considered the identification of three sources that a part of
538 the activity time of two of those sources coincide. The first source similar to the scenario 1 has
539 been considered at 8.75 km of the upstream end of the B2 and the other two sources considered
540 at 10 and 46 km of the upstream end of the B1. It is also assumed that the activity time of the
541 last two sources is after the end of the activity of the first source. In addition, it assumed that
542 part of the activity time of the sources that located at 10 and 46 km of the upstream end of the
543 B1 is simultaneous. This example is presented for two different cases in terms of the start
544 activity time of pollutant sources. Complementary explanations for each case are given below.

545 ### a) Test 1

546 In the first case, it is assumed that the source at 46 km of the upstream end of the B1 starts its
547 activity earlier than the source at 10 km of the upstream end of the B1(Figure 19). After
548 identification of the first source, similar to what described in the scenario 1, the forward model
549 is modified according to recovered source characteristics. After revising the forward model, a
550 comparison of observed and simulated data at the main stations (Figure 20), first shows a
551 difference between these two set of data at the M3 located at 57 km of the upstream end of the
552 B1. A few hours later, while the pollution cloud has not yet completely passed the M3, a
553 difference between the observed and simulated data at the M2 at 24 km of the upstream end of
554 the B1, is recognized. This means two sources are simultaneously active at upstream of these

two main stations. In order to correctly identify the suspect reaches to presence of these two sources, it is necessary to collect a concentration data at the instant of difference detection at all secondary stations between station M3 and M2 and the first main stations that located at upstream of them. Figure 21 (a) and (b) represent a comparison of observed and simulated data at sought secondary stations and at the instant of difference detection in M3 and M2, respectively.

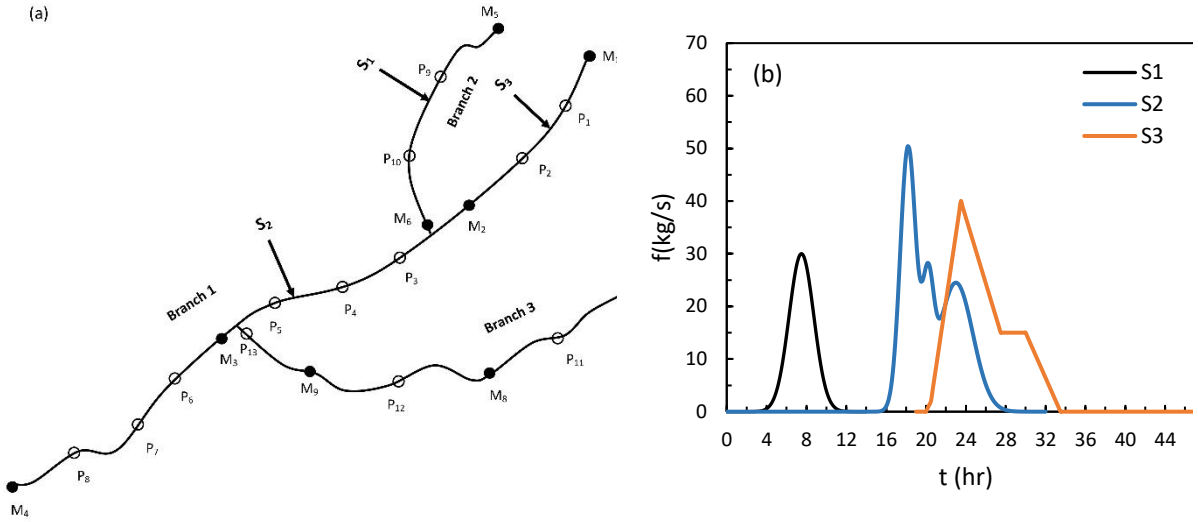

Figure 19- (a) location and (b) intensity function of pollutant sources (scenario 3-test 1)

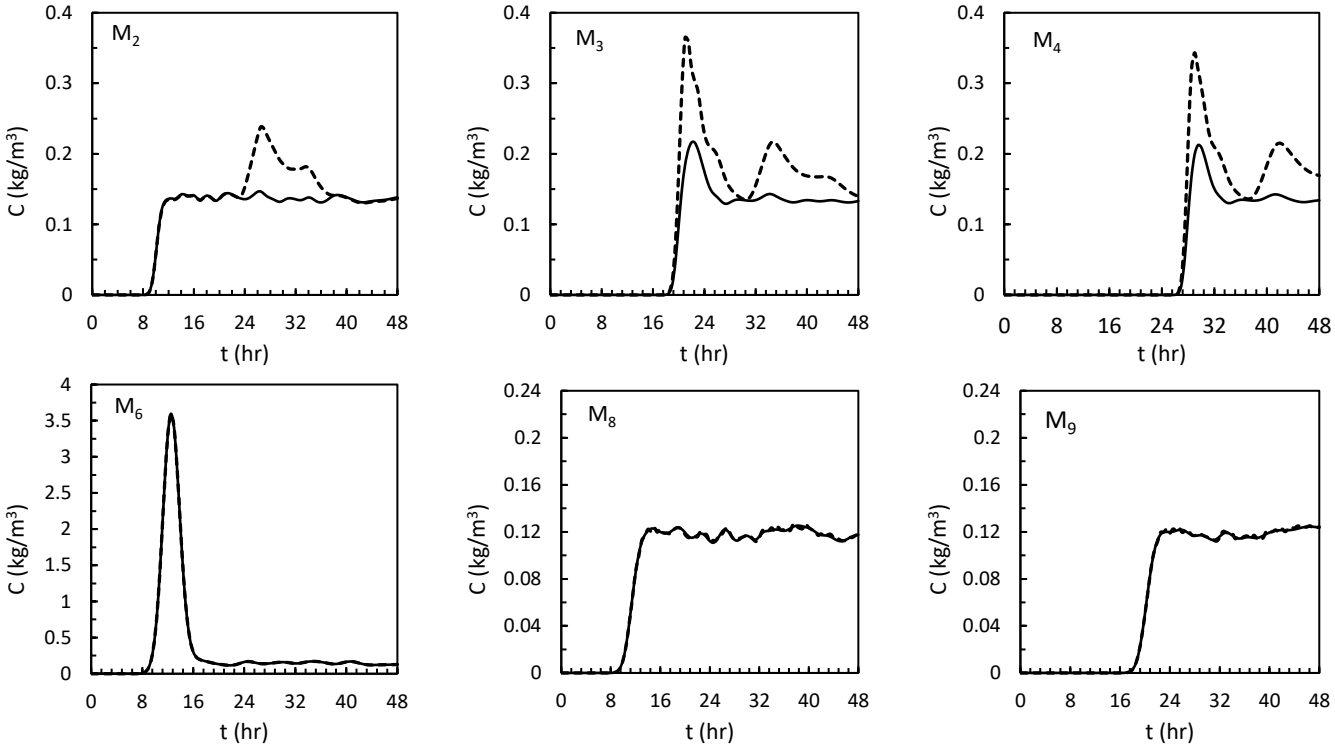

Figure 20- Comparison of simulated and observed data in main stations (scenario 3-test1) (solid line: simulated and dashed line: observed data)

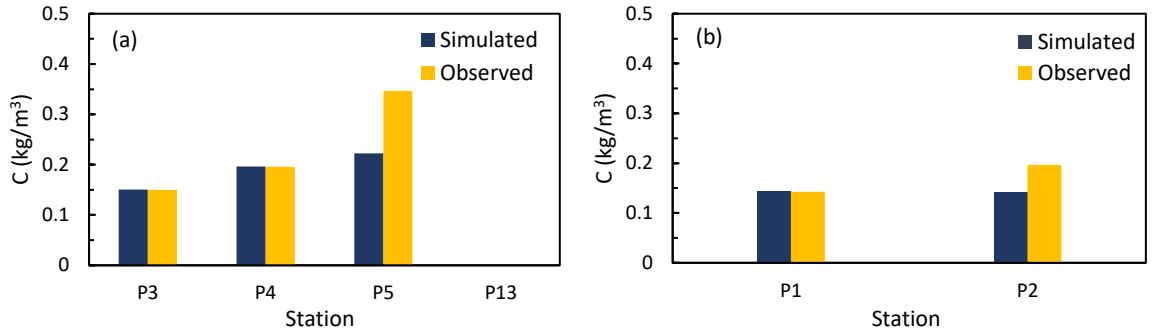

564 **Figure 21**- Comparison of simulated and observed data in secondary stations at the instant of
565 difference detection between the simulated and observed data in (a) M3 and (b) M2 (scenario 3-test1)

566 In addition, to ensure that there are no other active sources, the concentration-time data that
567 has been collected at secondary stations at the upstream and downstream of suspected reaches
568 are compared with simulated data. It should be noted that the beginning instant of data
569 collection is from the instant of difference detection at M3 and M2. Figure 22 shows a
570 comparison of observed and simulated data at secondary stations P1, P2, P4 and P5. As can be
571 seen from Figure 22, there is no difference between observed and simulated data at P1, which
572 means that there is no active source at upstream of that station during the activity of detected
573 source. A comparison of these two sets of data in P2 shows a difference. By comparing the
574 general form and peak concentration of C-t curve with C-t curve at M2 (Figure 20), it can be
575 deduced that this difference is due to the discovered source and there is no other active source.
576 Observed and simulated data at P4 and P5 also show difference. By a similar argument, it can
577 be concluded that this difference is due to the discovered sources and that there is no other
578 active source at upstream of these stations.

579 After determining the suspected reaches to presence of two sources, their exact location and
580 approximate intensity function are recovered using the spatial distribution of concentration data
581 in all downstream stations. Given that the source which located at 40 to 46 km of the upstream
582 end of the B1 has started its activity earlier, its exact location must be determined first. It
583 should be noted that this case is fundamentally different from the two previous two scenarios.
584 In the two previous scenarios, the spatial distribution of concentration data which used to
585 determine the exact location and approximate intensity function had been collected at the

instant of full passage of the pollution cloud from downstream secondary station. However, in this test, due to the simultaneous activity of two pollutant sources, the exact location and intensity function of the second pollutant source are determined using the spatial distribution of concentration data at the instant of discovering the effect of third source. This is because the observed data at the instant the full passage of pollutant cloud from the downstream secondary station represented the combined effects of two sources, and therefore using of them may lead to incorrect identification results. While at the instant of detection third source, its effect has not yet reached the downstream, and the data that has been recorded at downstream main and secondary stations shows only the effect of second source.

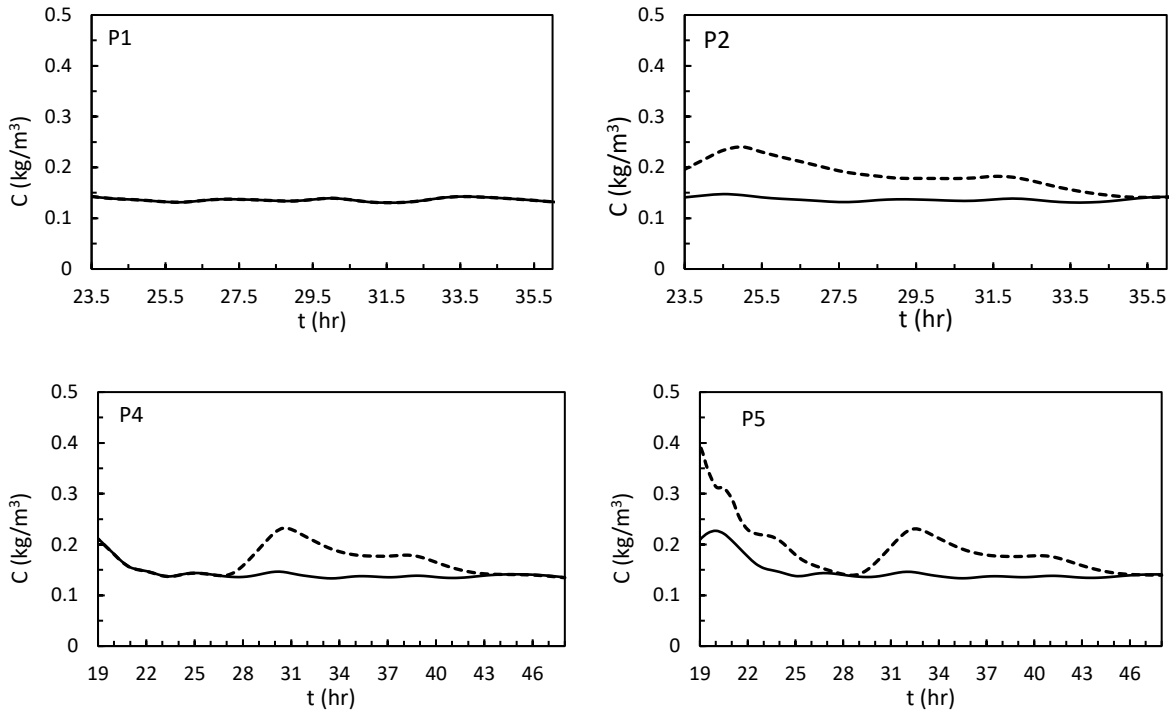

Figure 22- Comparison of observed and simulated data at secondary stations located at the upstream and downstream of suspected reaches during the period of permanent data collection by those stations (scenario 3-test 1) (solid line: simulated and dashed line: observed data)

The identification process is started by dividing the suspected reaches to presence of second and third sources into two equal length sub-reaches. Then, potential locations of the pollutant sources are considered in the center of those sub-reaches and by implementing the inverse model the exact location and approximate intensity function of each source is determined. Figure 23 shows the results of inverse model implementation for two potential locations for

second source, i.e. 42 and 46 km of the upstream end of the B1. As can be seen from it, a close to zero and a non-zero intensity functions have been obtained for 42 and 46 km potential locations, respectively. Therefore, it can be concluded that the second source of is located at 46 km of the upstream end of the B1, which corresponds to the assumed location. Subsequently, the location of third source is also determined using the spatial distribution of concentration data at the instant that pollutant cloud fully passes from P2. The results of the inverse model implementation for the two potential locations, i.e. 10 and 14 km of the upstream end of the B1, are shown in Figure 24. As indicated in this figure, a non-zero intensity function is obtained for the potential location of 10 km. So, it can be concluded that the third source is released at 10 km of the upstream end of the B1, which corresponds to the assumed location.

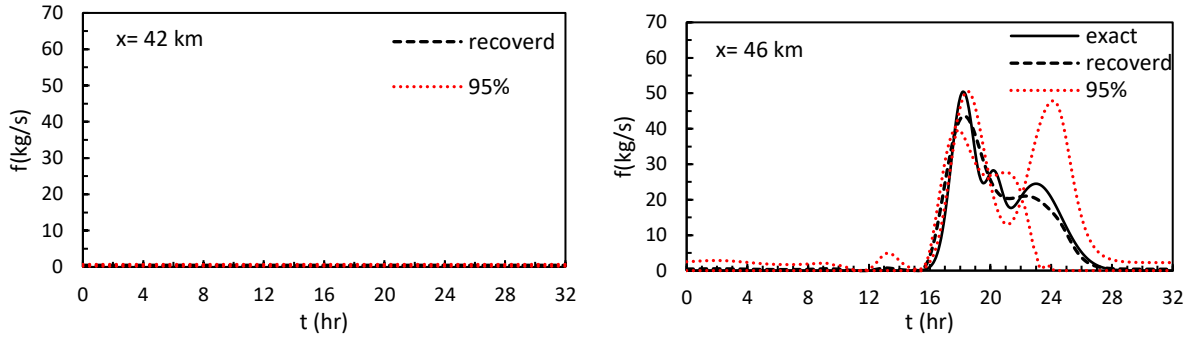

Figure 23- Recovered intensity function of S_2 at two potential locations using observed data at all main and secondary stations that located downstream of the suspected reach at the instant of recording the difference between the simulated and observed data in M2 (scenario 3-test1)

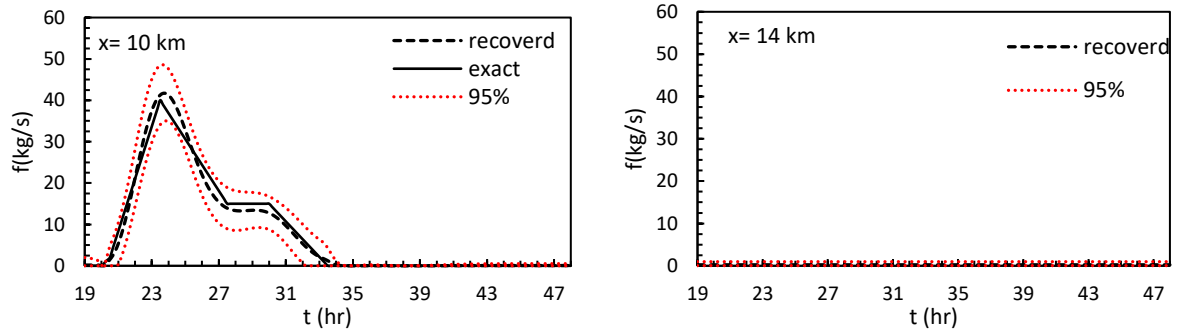

Figure 24- Recovered intensity function of S_3 at two potential locations using observed data at all main and secondary stations that located downstream of the suspected reach at the instant that the pollution cloud completely passes the P2 (scenario 3-test1)

Once the location of pollutant sources has been determined, their intensity functions should be recovered more accurately, assuming known source locations. Due to the simultaneous activity of two pollutant sources in this case, by starting from upstream, at first the exact

intensity function of the third pollutant source (located 10 km from upstream of B1) is retrieved using the concentration time data at M2. Then the forward model is modified, considering the obtained characteristics of this source. Thus, the C-t observed data at M3 will only include the effect of the second pollutant source ((located 46 km from upstream of B1)), and the exact intensity function of this source can also be calculated.

The results of the recovery of the third source intensity function using the C-t observed data at M2 are shown in Figure 25. Figure 26 shows the results of exact recovery of the intensity function of second source using the C-t observed data at M3 after deducting the effect of third source. The error indices for both approximate and exact recovery of the third source intensity function are given in Table 5. As can be seen from Figure 25 and Figure 26 and the error indices of Table 5, the accuracy of the results obtained using the c-t data is slightly better than the accuracy of the results obtained using the spatial distribution of concentration data. In addition, the 95% confidence interval width is narrower for the case of exact recovery, which indicates less uncertainty in obtained results in this case. The main reason for this is the difference in the number of observational data in these two cases. Since the spatial distribution of concentration data is usually sparse and the number of available data is much less than the number of desired instant for recovery of intensity function, the degree of uncertainty in retrieved results increases.

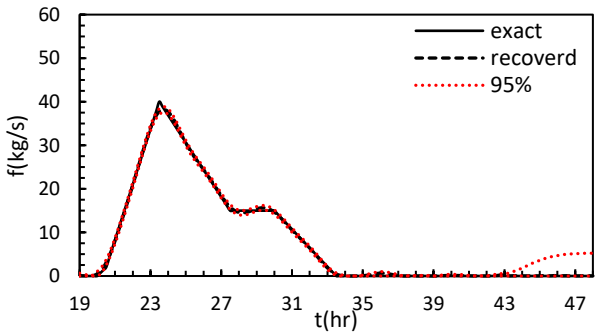

Figure 25- Recovered intensity function of S_3 by considering the exact location of the source and using observed concentration-time data at the first main station at downstream (M2)

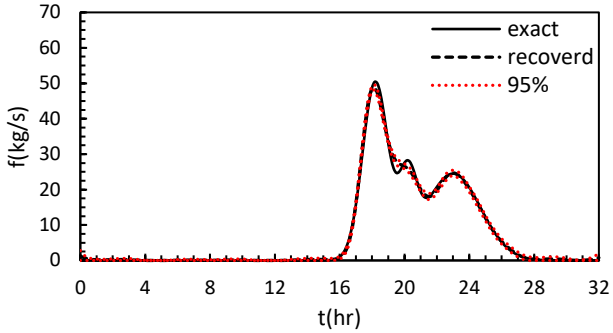

642 **Figure 26-** Recovered intensity function of S_2 by considering the exact location of the source and
643 using observed concentration-time data at the first main station at downstream (M3) and after revising
644 the forward model

645 **Table 5-** Error indices of scenario 3- test 1

Index	S_2 (46B1)		S_3 (10B1)	
	Recovery using spatial distribution of concentration data	Recovery using observed concentration-time data at the first main station at downstream (M3)	Recovery using spatial distribution of concentration data	Recovery using observed concentration-time data at the first main station at downstream (M2)
R^2 (%)	95.99	99.64	98.55	99.96
RMSE (kg/s)	2.4674	0.7477	1.5034	0.3585
MAE (kg/s)	1.4293	0.3975	0.9168	0.2196
de (kg/s)	184.7864	14.9453	92.1065	24.5408

646 ## b) Test 2

647 In the second case, it is assumed that the source at 10 km of the upstream end of the B1 starts
648 its activity earlier than the source at 46 km o the upstream end of the B1(Figure 27), which
649 creates a different condition in identification process than the first test. After identification of
650 the first source, similar to what described in the scenario 1, the forward model is modified
651 according to the recovered source characteristics. After revising the forward model, a
652 comparison of observed and simulated data at the main stations shows a difference between
653 these two set of data at the M2 located at 24 km of the upstream end of the B1 (Figure 28).

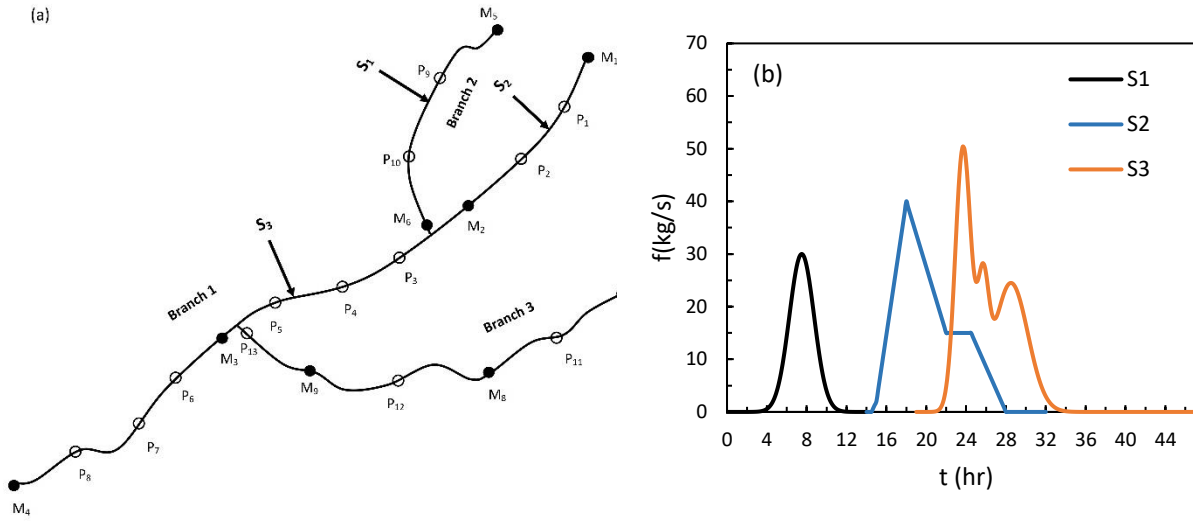

654 **Figure 27**- (a) location and (b) intensity function of pollutant sources (scenario 3-test 2)

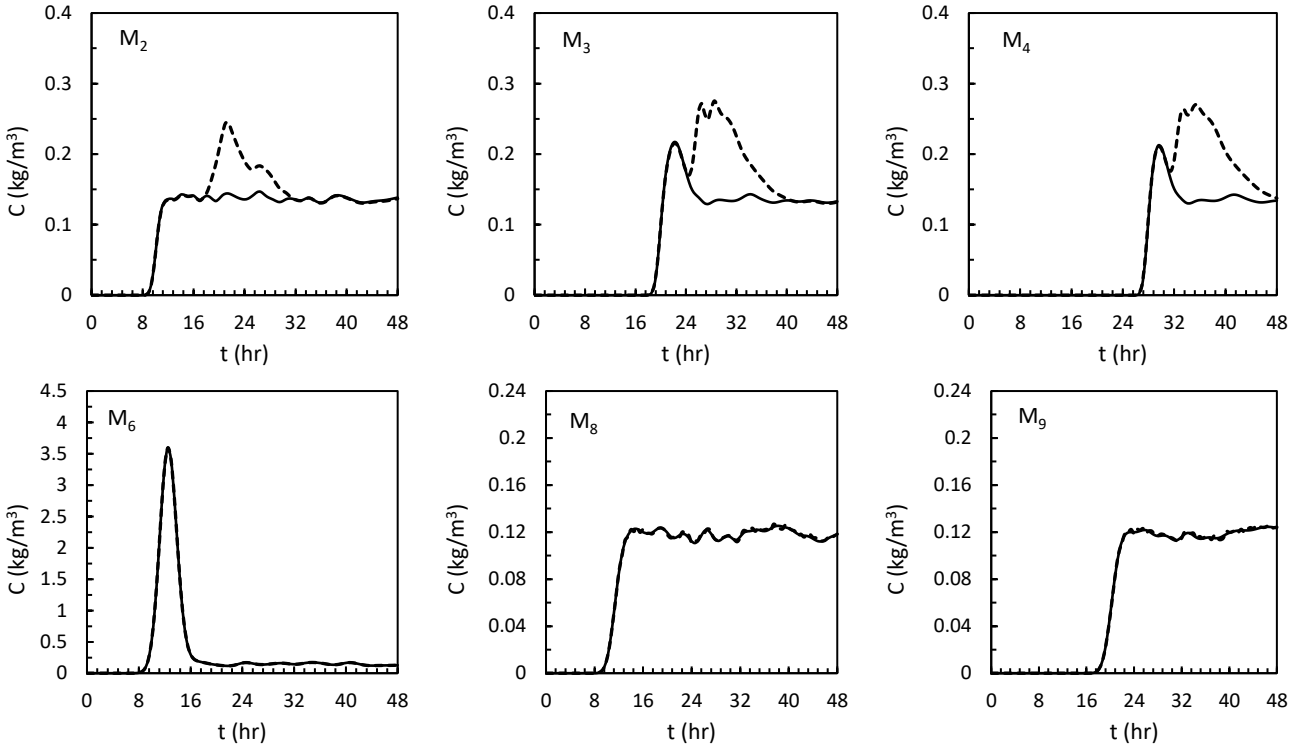

655 **Figure 28**- Comparison of simulated and observed data in main stations (scenario 3-test2) (solid line:
656 simulated and dashed line: observed data)

657 Once the difference between observed and simulated data sets was detected , it is necessary
658 to collect a concentration data at the instant of difference detection at all secondary stations
659 located between station M2 and the first main station at upstream (namely P1 and P2), and
660 compare those data with corresponding simulated data (Figure 29). According the Figure 29 It
661 can be deduced that the suspected reach to presence the second source is in between P1 and P2
662 (i.e. at 8 to 16 km of the upstream end of the B1). Also, in order to ensure that there are no

other simultaneously active sources upstream and downstream of the suspected reach, the observed and simulated data are compared at P1 and P2 during the permanent data recording period by these stations (Figure 30). As shown in Figure 30, there is no difference between the observed and simulated data at P1, which means that there is no active source upstream of suspected reach during the detection period. However, a comparison of these two sets of data in P2 shows a difference. Regarding the general form and peak concentration of observed C-t curve with the corresponding one at M2 (Figure 28), it can be inferred that this difference is due to the discovered pollutant source and there is no other active pollutant source.

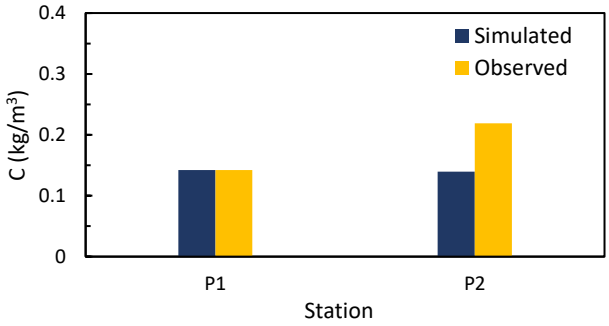

Figure 29- Comparison of simulated and observed data in secondary stations at the moment of difference detection between the simulated and observed data in M2 (scenario 3-test2)

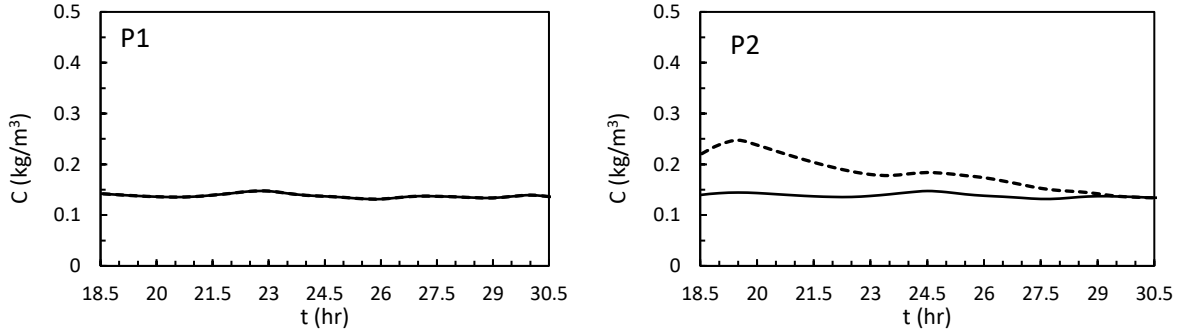

Figure 30- Comparison of observed and simulated data in secondary stations located at the upstream and downstream of suspected reach during the period of permanent data collection by those stations (scenario 3-test 2) (solid line: simulated and dashed line: observed data)

In the next step, the determined suspected reach is divided into two equal length sub-reaches of and the potential locations of the pollutant source is considered in the center of each of these sub-reaches, i.e. 10 and 14 km of the upstream end of the B1. Then, the inverse model is implemented using spatial distribution of concentration data at all station located at downstream of the suspected reach. The results of the inverse model implementation for both

potential locations are presented in Figure 31 .As indicated in figure, for a potential location of 14 km the intensity function is obtained close to zero, while for a potential location of 10 km a non-zero intensity is obtained. Therefore, it can be concluded that the second pollutant source is located at 10 km from upstream of the B1, which corresponds to the assumed location.

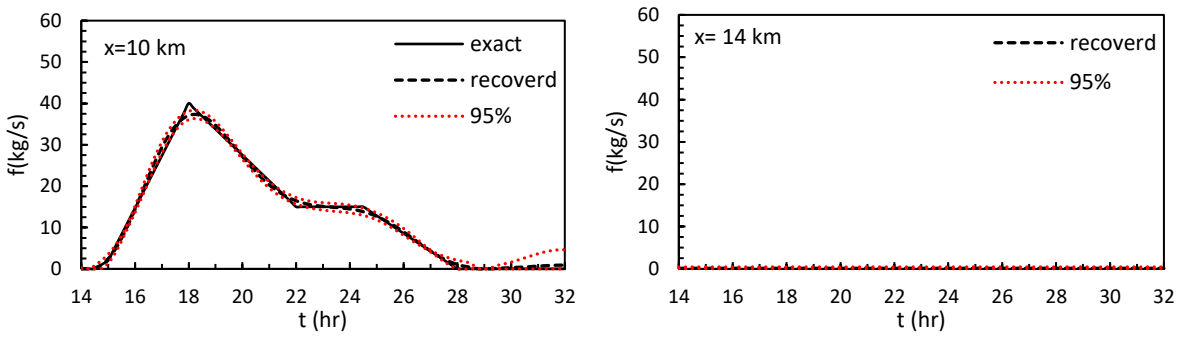

Figure 31- Recovered intensity function of S_2 at two potential locations using observed data at all main and secondary stations that located downstream of the suspected reach at the instant that the pollution cloud completely passes the P2 (scenario 3-test2)

After determining the exact location of the source, its intensity function are recovered more accurately, assuming the source location is known and using observed C-t data at M2 (Figure 32). The error indices for both approximate and exact recovery of the intensity function for second source are given in Table 6. As shown in Figure 32 and the error indices in Table 6, the accuracy of the results obtained using the C-t data is slightly better than the accuracy of the results obtained using the concentration spatial series data and the 95% confidence interval width is narrower as well. So, uncertainty associated with retrieved results are less in this case. The main reason for this is availability of more observation data compare to the case of recovery with spatial distribution of concentration data.

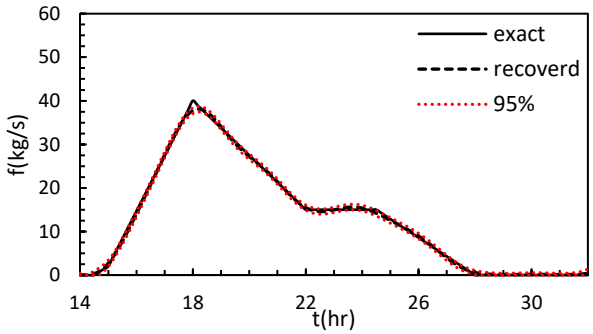

Figure 32- Recovered intensity function of S_2 by considering the exact location of the source and using observed concentration-time data at the first main station at downstream (M2)

After identification the characteristics of the second pollutant source, the forward model is modified according to determined characteristics and the observed and simulated data that obtained by modified forward model are compared. Comparison of these two sets of data indicates the existence of difference at the M3 (Figure 33). Therefore, it can be concluded that a pollution source is active upstream of this station. By comparing the concentration data at the instant of difference detection in all secondary stations that located between the M3 and the first main station at upstream (M2) (Figure 34), the suspected reach to presence the third pollutant source is determined between 40 to 48 km of the upstream end of the B1.

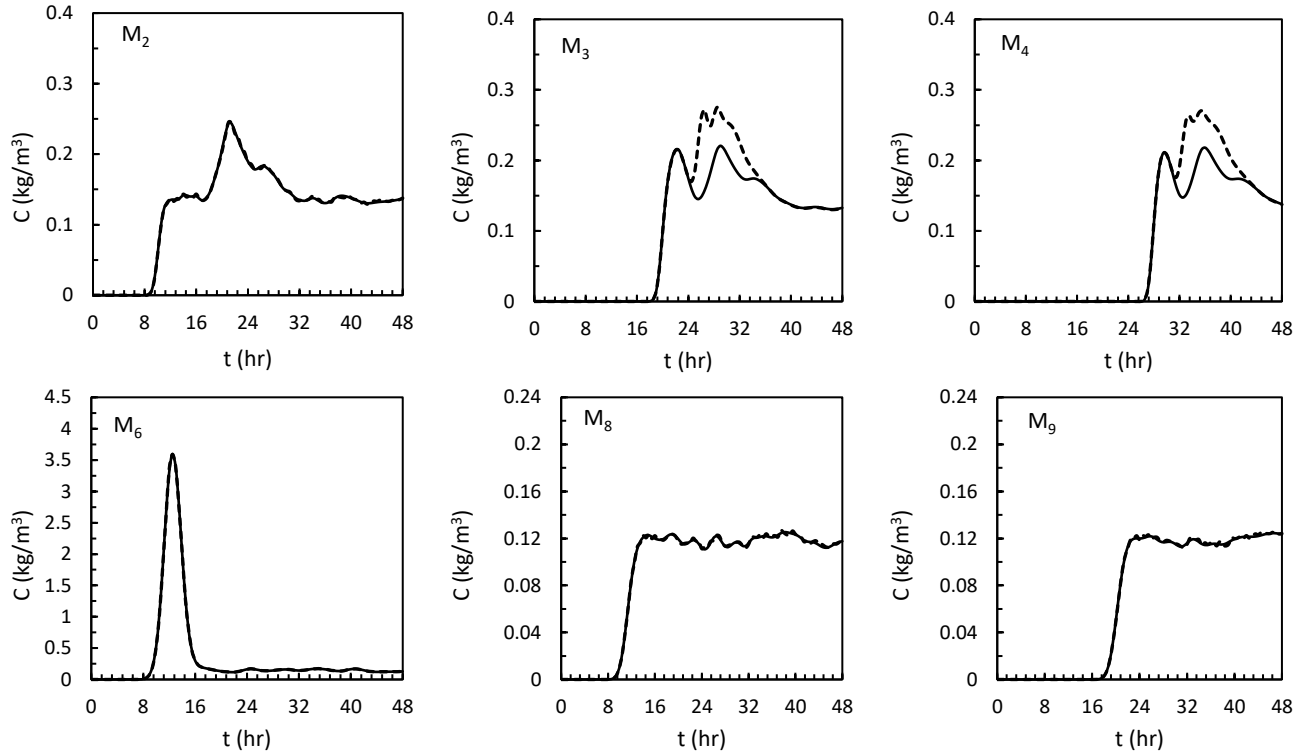

Figure 33- Comparison of simulated and observed data in main stations (scenario 3-test2) after identification of S_2 and revising the forward model (solid line: simulated and dashed line: observed data)

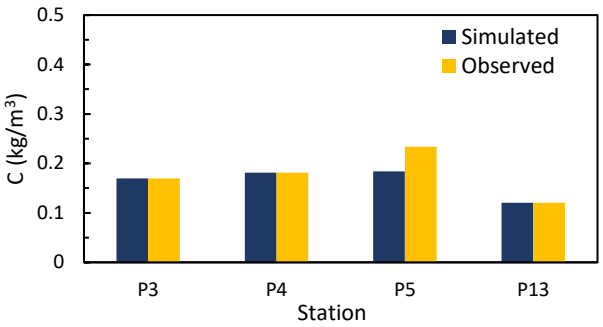

712 **Figure 34**- Comparison of simulated and observed data in secondary stations after identification of S_2
713 and at the instant of difference detection between the simulated and observed data in M3 (scenario 3-
714 test2)

715 In order to ensure that there are no other simultaneously active sources at upstream and
716 downstream of the suspected reach, the observed and simulated data at P4 and P5 secondary
717 stations are compared during the permanent data recording period by these stations(Figure 35).
718 As can be seen from Figure 35 there is no difference between the observed and simulated data
719 at P4, which means that there are no other active sources during the identification period. A
720 comparison of these two sets of data in the P5 shows the difference. By comparing the general
721 form and peak concentrations of Observed C-t curve with the associated one at M3 (Figure 33),
722 it can be argued that this difference is due to the discovered contaminant source and there are
723 no other active sources.

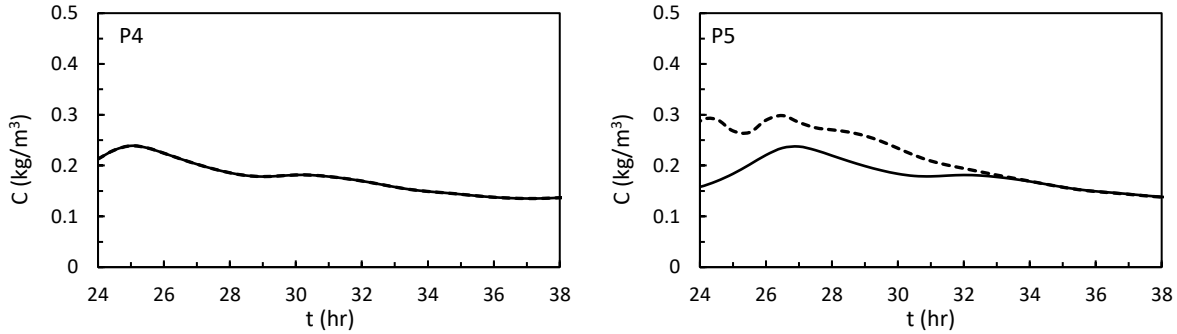

724 **Figure 35-** Comparison of observed and simulated data in secondary stations located at the upstream
725 and downstream of suspected reach to presence of S_3 during the period of permanent data collection
726 by those stations (scenario 3-test 2) (solid line: simulated and dashed line: observed data)

727 In the next step, the exact location and approximate intensity function of the third source
728 are recovered by implementation inverse model for two potential source locations which are in
729 the center of two equal length sub-reaches, i.e. 42 and 46 km of the upstream end of the B1.
730 The results have been presented in Figure 36 that shows that the location of the third source

must be at 46 km of the upstream end of the B1, for which a non-zero intensity function had been obtained. However, as shown in this figure, there is no good match between the recovered and the exact intensity function. The reason for this is the time delay in identifying the effect of the third pollutant source at M3, due to the synchronization of its activity with the second pollutant source. As a result, some part of information about the third source of the pollutant is lost and consequently retrieval accuracy had been reduced and associated uncertainty increased.

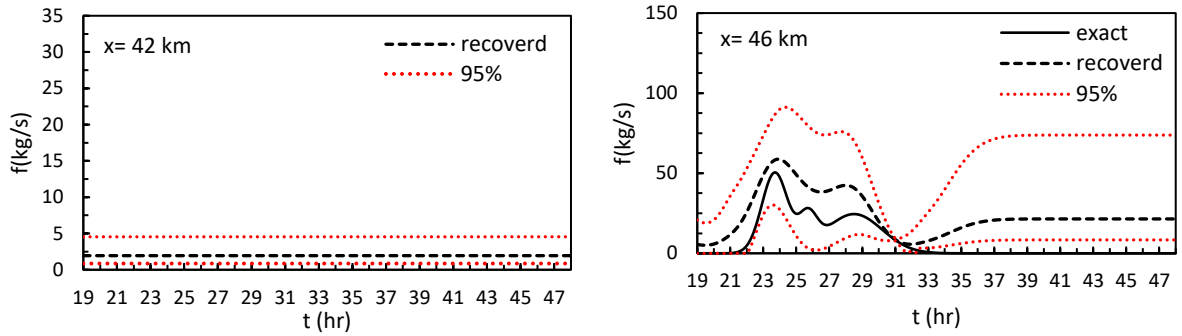

Figure 36- Recovered intensity function of S_3 at two potential locations using observed data at all main and secondary stations that located downstream of the suspected reach at the instant of recording the difference between the simulated and observed data in M3 (scenario 3-test2)

After determining the exact location of the third pollutant source, its intensity function is retrieved more accurately using the C-t data at M3 (Figure 37). As it is clear from the figure, the model has succeeded in recovering the intensity function of the mentioned pollutant source with good and acceptable accuracy. The error indices presented in Table 6also confirm this.

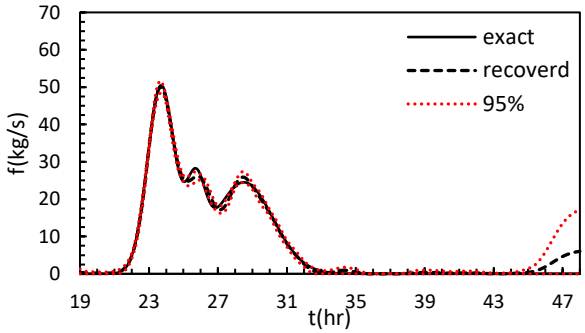

Figure 37- Recovered intensity function of S_3 by considering the exact location of the source and using observed concentration-time data at the first main station at downstream (M3) and after revising the forward model

751 **Table 6-** Error indices of scenario 3- test 2

Index	S_2 (10B1)		S_3 (46B1)	
	Recovery using spatial distribution of concentration data	Recovery using observed concentration-time data at the first main station at downstream (M2)	Recovery using spatial distribution of concentration data	Recovery using observed concentration-time data at the first main station at downstream (M3)
R^2 (%)	99.61	99.88	74.0750	98.92
RMSE (kg/s)	0.7702	0.4162	17.4011	1.3823
MAE (kg/s)	0.5797	0.3057	15.9637	0.7126
de (kg/s)	20.8116	11.716	741.1620	52.0625

752 # 4. Conclusion

753 This study has been presented an innovative multistep method for simultaneous identification
754 of the number, location and release history of pollutant source in a river network considering
755 unsteady and non-uniform flow. The only priori information that the method needs are the
756 expected activity period for recovery, accuracy of spatial range for retrieval the source location
757 and the travel time of each branch. Based on those priori information, at first an adaptive
758 arrangement of observation points is proposed. Then suspect reaches to presence of pollutant
759 sources are delineate by comparing the simulated and observed breakthrough curves at
760 considered stations. In this step, the number of all simultaneous active pollution sources is also
761 determined. Then, the suspected reaches are divided to some sub-reaches and it is assumed that
762 the origin of possible sources is in the center of those sub- reaches. At the second step the
763 location and approximate release history of pollution sources are recovered by means of a
764 geostatistical approach, that considered simultaneously all the possible candidates. The source
765 location is considered as the location where the highest amount of released pollutant is
766 estimated. Finally, the exact release history is determined using the temporal distribution of
767 observed concentration data at the first downstream main station.

768 The proposed method is suitable for practical applications, since it is based on one-
769 dimensional flow and transport models and considers the complicated real-world conditions.
770 The method is effective and easy to apply in complex river networks as well as single-branch

ones. Moreover, since in each simulation it is possible to identify all active pollutant sources, the required computational time is significantly lower than common iterative methods such as simulation-optimization approach. Another significant advantage of the proposed method is that it provides unique results for sought characteristics, using minimum observational data. In fact, if the observation points placed based on suggested pattern, obtaining the unique results is guaranteed. The results of application of method to a hypothetical river network for different scenarios in terms of the number, release time and location of pollutant sources, showed that the methodology performs very well in case of large-scale river networks. The given results were acceptable regarding to a limited requirement inputs. Of course, the quality of the recovery is dependent on the accuracy of the observation data. So, the uncertainty associated with results due to using erroneous observational data, was considered also through 95 percent confidence interval. This paper is one of the first attempts to solve the complicated and ill-posed problem of simultaneous identification of all characteristics of multiple pollutant sources in a complex river network. There are several aspects that need further investigation. Currently, the application of proposed method is limited to cases in which the activity time of pollutant sources are equal to or greater than expected activity time for recovery. Some measures such as considering random data collecting in secondary station might alleviate this problem. This is a subject for our future study.

References

Andrle, M. and El Badia, A. 2012. Identification of multiple moving pollution sources in surface waters or atmospheric media with boundary observations. *Inverse problems,* 28**,** 075009.

Atmadja, J. and Bagtzoglou, A. C. 2001. State of the art report on mathematical methods for groundwater pollution source identification. *Environmental forensics,* 2**,** 205-214.

Boano, F., Revelli, R. and Ridolfi, L. 2005. Source identification in river pollution problems: A geostatistical approach. *Water resources research,* 41.

Box, G. E. and Cox, D. R. 1964. An analysis of transformations. *Journal of the Royal Statistical Society: Series B (Methodological),* 26**,** 211-243.

Butera, I., Tanda, M. G. and Zanini, A. 2013. Simultaneous identification of the pollutant release history and the source location in groundwater by means of a geostatistical approach. *Stochastic Environmental Research and Risk Assessment,* 27**,** 1269-1280.

Chapra, S. C. (2008). Surface water-quality modeling. Illinois: Waveland press.

Cheng, W. P. and Jia, Y. 2010. Identification of contaminant point source in surface waters based on backward location probability density function method. Advances in Water Resources, 33, 397-410.

De Marsily, G. 1986. Quantitative Hydrogeology: Groundwater Hydrology for Engineers Academic Press. *Inc., Orlando, Florida*.

El Badia, A. and Hamdi, A. 2007. Inverse source problem in an advection-dispersion-reaction system: application to water pollution. *Inverse Problems,* 23**,** 2103.

Fischer, H. B., Koh, R. C., Brooks, N. H., list, E. J. and Imberger, J. 1979. Mixing in Inland and Coastal Waters. Academic Press.

Ghane, A., Mazaheri, M. and Samani, J. M. V. 2016. Location and release time identification of pollution point source in river networks based on the Backward Probability Method. *Journal of environmental management,* 180**,** 164-171.

Gzyl, G., Zanini, A., Frączek, R. and Kura, K. 2014. Contaminant source and release history identification in groundwater: a multi-step approach. *Journal of contaminant hydrology,* 157**,** 59-72.

Hadamard, J. 1923. Lectures on Cauchy's Problem in Linear Partial Differential Equations, Yale University Press.

Hamdi, A. 2009. The recovery of a time-dependent point source in a linear transport equation: application to surface water pollution. Inverse Problems, 25, 075006.

Hamdi, A. 2016. Detection-Identification of multiple unknown time-dependent point sources in a 2 D transport equation: application to accidental pollution. Inverse Problems in Science and Engineering, 1-25.

Hoeksema, R. J. and Kitanidis, P. K. 1985. Comparison of Gaussian conditional mean and kriging estimation in the geostatistical solution of the inverse problem. Water Resources Research, 21, 825-836.

Jiang, H. 2008. Adaptive feature selection in pattern recognition and ultra-wideband radar signal analysis. California Institute of Technology.

Kitanidis, P. K. 1995. Quasi-linear geostatistical theory for inversing. *Water resources research,* 31**,** 2411-2419.

Kitanidis, P. K. 1996. On the geostatistical approach to the inverse problem. *Advances in Water Resources,* 19**,** 333-342.

Kitanidis, P. K. and Shen, K.-F. 1996. Geostatistical interpolation of chemical concentration. *Advances in Water Resources,* 19**,** 369-378.

Lee, Y. J., Park, C. and Lee, M. L. 2018. Identification of a Contaminant Source Location in a River System Using Random Forest Models. *Water,* 10**,** 391.

Liu, C. and Ball, W. P. (1999). Application of inverse methods to contaminant source identification from aquitard diffusion profiles at Dover AFB, Delaware. Water Resources Research, 35, 1975-1985.

Mazaheri, M., Mohammad Vali Samani, J. and Samani, H. M. V. 2015. Mathematical Model for Pollution Source Identification in Rivers. *Environmental Forensics,* 16**,** 310-321.

Michalak, A. M. 2002. Environmental Contamination with Multiple Potential Sources and the Common Law: Current Approaches and Emerging Opportunities. Fordham Environmental Law Journal, 14, 147-206.

Michalak, A. M. and Kitanidis, P. K. 2002. Application of Bayesian inference methods to inverse modelling for contaminants source identification at Gloucester Landfill, Canada. DEVELOPMENTS IN WATER SCIENCE, 47, 1259-1266.

Michalak, A. M. and Kitanidis, P. K. 2003. A method for enforcing parameter nonnegativity in Bayesian inverse problems with an application to contaminant source identification. *Water Resources Research,* 39.

Michalak, A. M. and Kitanidis, P. K. 2004a. Application of geostatistical inverse modeling to contaminant source identification at Dover AFB, Delaware. *Journal of hydraulic research,* 42**,** 9-18.

Michalak, A. M. and Kitanidis, P. K. 2004b. Estimation of historical groundwater contaminant distribution using the adjoint state method applied to geostatistical inverse modeling. *Water Resources Research,* 40.

Morrison, R. D. 2000a. Critical Review of Environmental Forensic Techniques: Part I. *Environmental Forensics,* 1**,** 157-173.

Morrison, R. D. 2000b. Critical review of environmental forensic techniques: Part II. *Environmental Forensics,* 1**,** 175-195.

Neupauer, R. M., Borchers, B. and Wilson, J. L. 2000. Comparison of inverse methods for reconstructing the release history of a groundwater contamination source. *Water Resources Research,* 36**,** 2469-2475.

Skaggs, T. H., and Z. J. Kabala. (1994). Recovering the release history of a groundwater contaminant. *Water Resour. Res, 30(1)*, 71– 79.

Skaggs, T. H. and Kabala, Z. 1998. Limitations in recovering the history of a groundwater contaminant plume. *Journal of Contaminant Hydrology,* 33**,** 347-359.

Snodgrass, M. F. and Kitanidis, P. K. 1997. A geostatistical approach to contaminant source identification. *Water Resources Research,* 33**,** 537-546.

Taylor, G. 1954. The dispersion of matter in turbulent flow through a pipe. *Proceedings of the Royal Society of London. Series A. Mathematical and Physical Sciences,* 223**,** 446-468.

Telci, I. T. and Aral, M. M. 2011. Contaminant source location identification in river networks using water quality monitoring systems for exposure analysis. *Water Quality, Exposure and Health,* 2, 205-218.

Wang, J., Zhao, J., Lei, X. and Wang, H. 2018. New approach for point pollution source identification in rivers based on the backward probability method. Environmental Pollution, 241, 759-774.

Woodbury, A., Sudicky, E., Ulrych, T. J. and Ludwig, R. 1998. Three-dimensional plume source reconstruction using minimum relative entropy inversion. Journal of Contaminant Hydrology, 32, 131-158.

Wu, W. 2007. *Computational river dynamics*, CRC Press.

Yang, H., Shao, D., Liu, B., Huang, J. and Ye, X. 2016. Multi-point source identification of sudden water pollution accidents in surface waters based on differential evolution and Metropolis–Hastings–Markov Chain Monte Carlo. *Stochastic environmental research and risk assessment,* 30**,** 507-522.

Declarations

Funding

No funding was received for conducting this study.

Conflicts of interest/Competing interests

The authors declare that they have no conflicts of interest.

Availability of data and material

Not applicable.

Code availability

Not applicable.